

Novel elastic instability of amorphous solids in finite spatial dimensions

Masanari Shimada,^{1,*} Hideyuki Mizuno,¹ and Atsushi Ikeda^{1,2}

¹*Graduate School of Arts and Sciences, The University of Tokyo, Tokyo 153-8902, Japan*

²*Research Center for Complex Systems Biology, Universal Biology Institute,
The University of Tokyo, Tokyo 153-8902, Japan*

(Dated: September 2, 2020)

Recent progress has advanced the understanding of anomalous vibrational excitations in amorphous solids. In the lowest-frequency region, the vibrational spectrum follows a non-Debye quartic law, which persists up to zero frequency without any frequency gap. This gapless vibrational density of states (vDOS) suggests that glasses are on the verge of instability. This feature of marginal stability is now highlighted as a key concept in the theories of glasses. In particular, the elasticity theory based on marginal stability predicts the gapless vDOS. However, this theory yields a quadratic law, *not* the quartic law. To address this inconsistency, our preceding paper [M. Shimada, H. Mizuno, and A. Ikeda, *Soft Matter*, **16**, 7279, 2020] presented a new type of instability, which is different from the well-established, conventional one and proposed that amorphous solids are marginally stable in the sense of the former. In this paper, we report further extended and detailed results for these instabilities. Through the analyses of various examples of disorder, we demonstrate that real glasses in finite spatial dimensions can be marginally stable by this novel instability.

I. INTRODUCTION

Lattice vibrations of crystals, called phonons, can be fully described in terms of the spatial periodicity and defects [1]. The transportation of phonons controls the thermal properties, whereas structural defects cause mechanical failure. In contrast, amorphous solids have no periodicity in their structures, and it is impossible to define defects unambiguously. Indeed, in amorphous solids, two species of anomalous vibrational modes have been observed in addition to phonons, even in the low-frequency region, where we can safely apply the Debye theory to crystals [2–6]. The first species are heterogeneous and spatially extended vibrations. They manifest as a peak at round 1 THz in the vibrational density of states (vDOS) $g(\omega)$ divided by the squared frequency ω^2 , referred to as the boson peak (BP) [2]. The second species are strongly anharmonic [7, 8] and spatially localized vibrations referred to as quasilocalized vibrations (QLVs). These vibrational modes control the low-temperature thermal properties of glasses [9–15]. In particular, because the frequency of the QLVs is much lower than the BP frequency, they affect mechanical failure [16–18] under a load as well as the structural relaxation of supercooled liquids near the glass transition temperature [19, 20]. For these reasons, the anomalous vibrations of glasses have attracted broad interest in the past decades.

Recent extensive numerical studies have reported the quantitative properties of these anomalous vibrations. Simulations using weakly coordinated jammed packings near the jamming transition [21] have established that the vDOS obeys a power-law dependence, $g(\omega) \sim \omega^2$, at approximately the BP frequency. This scaling is independent of the spatial dimension d , which is distinct from the

Debye law, $g_{\text{Debye}}(\omega) \sim \omega^{d-1}$, and is referred to as the non-Debye scaling law. Numerical studies further suggested that this scaling can persist even in Lennard–Jones glasses [22] far from the jamming transition in large spatial dimensions [23].

The non-Debye scaling law, however, does not extend down to zero frequency; instead, the coexistence of phonons and QLVs emerges below the BP frequency [24–26]. The QLVs consist of a core and a far field that decays algebraically in space if they are not hybridized with phonons [24, 27]. This decay is sufficiently rapid for their participation ratio to scale as $1/N$ like truly localized vibrations, where N is the number of particles. A numerical study established that the motions of particles in the cores are energetically unstable, which are stabilized by the far-field components [28]. Moreover, the QLVs are similar to the response to a local dipolar force [28–31], and their characteristic frequency increases rapidly as the glass transition is approached, together with a measure of elastic stiffness based on the local response [31]. The vDOS of the QLVs follows another power law, $g_{\text{QLV}}(\omega) \sim \omega^\beta$, where usually $\beta = 4$ [24, 25, 32], but when one prepares glasses by quenching liquids at sufficiently high temperatures, $\beta \simeq 3$ [32]. Here, a significant point of this vDOS is that this power law persists at zero frequency. That is, the vDOS of the QLVs is *gapless*, whereas the non-Debye scaling law is *gapped* in finite dimensions.

The gapless nature of the QLVs is strongly reminiscent of the marginal stability of glasses [33]. Amorphous systems are susceptible to infinitesimal perturbations such as shear deformation and thermal agitation. A numerical study on the yielding transition found that glasses yield under infinitesimally small strains in the thermodynamic limit [34]. Similarly, intermittent rearrangements are induced in glasses by infinitesimal thermal energy [35].

This marginality of glasses can be rationalized as follows [33, 36]. Generally, the configurational space ex-

* masanari-shimada444@g.ecc.u-tokyo.ac.jp

plored by a system can be divided into three pieces in terms of the stability of elementary excitations: absolutely stable, unstable, and marginally stable configurations [33, 36]. When we perturb an absolutely stable configuration, it is forced to return to the initial point by restoring forces, whereas an unstable configuration moves away from the initial point [33, 36]. The marginally stable phase exists between the two phases [33, 36]. Specifically for particulate systems, normal liquids are unstable and frequently undergo structural relaxations, whereas crystals are absolutely stable. Unlike crystals, glasses are predicted to be marginally stable from a dynamical point of view. When we prepare glasses, we usually quench normal liquids. First, the dynamics are driven by unstable excitations, and structural relaxations occur. When the system approaches the stable phase, the number of unstable excitations decreases, and when it attains marginal stability, the dynamics freezes [33, 36]. Significantly, the marginal stability requires low-energy gapless excitations [33], which may be identified as QLVs in the case of glasses. [37].

In light of the notion of marginal stability, several attempts have been made to describe the low-frequency vibrations of glasses [38–44]. Among them, we focus on the elasticity theory with quenched disorder [38–41]. The theory analyzes the elasticity model, either a coarse-grained continuum [38, 39] or a spring network [40, 41], with spatially fluctuating stiffness. It has succeeded in reproducing several vibrational properties of glasses, such as the non-Debye scaling law around the BP frequency [39, 41]. In particular, when the theory is applied to jammed systems [40, 41, 45, 46], it reproduces several power law exponents [47–50] by utilizing the marginal stability of amorphous solids.

However, this elasticity theory predicts that the non-Debye scaling becomes gapless when the system is marginally stable [41]. This is severely inconsistent with the abovementioned numerical observations. To reconcile the theory with the numerical data, it has been argued that real glasses are almost, but not exactly, marginally stable [41]. At any rate, however, the theory cannot reproduce the vDOS of the QLVs, $g_{\text{QLV}}(\omega) \sim \omega^\beta$; instead, it illustrates the gapped non-Debye scaling law and the Debye law $g_{\text{Debye}}(\omega) \sim \omega^{d-1}$ in the zero-frequency limit.

The replica theory for the perceptron [42] also predicts gapless non-Debye scaling, similar to the elasticity theory. Recently, a phenomenological attempt has been proposed to reproduce the QLVs by introducing spatial fluctuations in the distance from the marginal stability [43, 44].

All previous studies therefore concluded that real glasses are almost, but not exactly, marginally stable [41, 43, 44]. That is, the theory captures the nature of the mechanical instability, whereas the remaining task is to locate the system correctly in the configuration space. In contrast, we proposed, in the preceding paper [51], another mechanism for the instability, referred to as local instability, as an alternative to the previous

interpretation within the framework of the elasticity theory with quenched disorder. The physical picture of this overlooked instability is fully consistent with those of the QLVs, and we presented a toy model that reproduces the gapless quartic law of the vDOS $g(\omega) \sim \omega^4$ when the system is marginally stable owing to local instability. Our results strongly suggest that real glasses are marginally stable, not in the sense of the conventional instability resulting in gapless non-Debye scaling, but rather in the sense of local instability.

In this study, we will present an extended and thorough analysis of the local instability using the simplest elasticity model. In contrast to the preceding study [51], we present several specific examples before the main general argument. Although the derivation of the local instability is the same as in the preceding study, we can obtain useful insights from those examples. After introducing the local instability, we present new analytical and numerical calculations, which were not reported in the preceding paper. In particular, we illustrate that when the system is marginally stable, some classes of stiffness distributions yield a gapless vDOS following $g(\omega) \sim \omega^{2\nu+1}$, where $\nu > 1$ is an exponent of the distributions.

The remainder of this paper is organized as follows. The first part, Section II, analyzes the scalar displacement model (SDM) [52]. In Section II A, we introduce the details of the model, and in Section II B, we apply an approximation referred to as the effective medium approximation (EMA) to the model. In Section II C, we discuss the large dimension limit of this model, in which the EMA becomes exact [53]. We introduce conventional instability in this section. In Sections II D and II E, we investigate specific types of disorder, thus reporting contrasting results. Based on these results, we introduce the local instability and related conditions in Section II F. In Section II G, we present a series of disorders that illustrate both conventional and local instabilities. Finally, we derive the vDOS when the system is marginally stable in terms of the local instability in Section II H. The second part, Section III, treats the vector displacement model (VDM), which has been analyzed in the preceding paper [51] and in Refs. [40, 45]. This is almost equivalent to the model of the first part. Thus, after introducing the model in Section III A, we describe only the differences from the preceding sections in Section III B. In Section III C, we present a class of models that yield continuously vanishing elastic stiffness in relation to the recent numerical results of jammed systems [54]. Finally, we summarize the results and discuss their implications in Section IV.

II. SCALAR DISPLACEMENT MODEL

A. Model

To study the vibrations of glasses, we first consider the SDM [52, 55]. The model is a d -dimensional simple cubic lattice of N elements with unit mass and scalar displacements $\{u_i\}_{i=1}^N$. Each nearest-neighbor pair $\langle ij \rangle$ is connected by a spring whose stiffness k_{ij} is an independent random variable obeying the probability distribution $P(k_{ij})$.

Therefore, the equation of motion is

$$\frac{d^2}{dt^2} u_i = - \sum_{\langle ij \rangle} k_{ij} (u_i - u_j). \quad (1)$$

Using the bra-ket notation,

$$\frac{d^2}{dt^2} |u\rangle = -\hat{\mathcal{M}} |u\rangle, \quad (2)$$

where

$$\begin{aligned} \hat{\mathcal{M}} &= \sum_{\langle ij \rangle} k_{ij} (|i\rangle - |j\rangle)(\langle i| - \langle j|), \\ &\equiv \sum_{\alpha=\langle ij \rangle} k_\alpha |\alpha\rangle \langle \alpha|. \end{aligned} \quad (3)$$

is the dynamical matrix. This is one of the simplest elasticity models. When we replace the equation of motion with a master equation, we obtain a model for the hopping transport of charge carriers in a disordered semiconductor [52].

The mean of the distribution, $\mu \equiv \overline{k_{ij}} = \int dk_{ij} k_{ij} P(k_{ij})$, must be positive. It should be noted that our model should be considered as a coarse-grained model, and thus the effects of microscopic stress and frustration are encoded as negative stiffness [56, 57]. Therefore, the negative stiffness is the source of the instability, or, conversely, no instability occurs when all the springs possess positive stiffness.

Green's function for Eq. (2) is defined as $\hat{\mathcal{G}}(\omega) \equiv (\hat{\mathcal{M}} - \omega^2)^{-1}$. When all springs have the same stiffness K , we can derive Green's function for such a homogeneous system as

$$\begin{aligned} G_K(\mathbf{r}_{ij}, \omega) &\equiv \langle i | \hat{\mathcal{G}}_K(\omega) | j \rangle \\ &= \int_{\mathbf{q} \in [-\pi, \pi]^d} \frac{d\mathbf{q}}{(2\pi)^d} \frac{e^{i\mathbf{q} \cdot \mathbf{r}_{ij}}}{K \sum_{m=1}^d (2 - 2 \cos q_m) - \omega^2}, \quad (4) \\ &\rightarrow \int_{\mathbf{q} \in [-\pi, \pi]^d} \frac{d\mathbf{q}}{(2\pi)^d} \frac{e^{i\mathbf{q} \cdot \mathbf{r}_{ij}}}{K q^2 - \omega^2} \quad (q \ll 1). \end{aligned}$$

where \mathbf{r}_{ij} is a vector from the i th element to the j th element, and we have used the long-wavelength limit in the last line.

B. Effective medium approximation

In this section, we introduce the EMA, as in Ref. [40, 41, 52]. It yields an approximate disorder-averaged

Green's function $\overline{\hat{\mathcal{G}}(\omega)}$ within a mean-field-like approach. We decompose the dynamical matrix as follows:

$$\begin{aligned} \hat{\mathcal{M}} - \omega^2 &= \sum_{\alpha=\langle ij \rangle} k_\alpha |\alpha\rangle \langle \alpha| - \omega^2, \\ &= \left[k_{\text{eff}}(\omega) \sum_{\alpha=\langle ij \rangle} |\alpha\rangle \langle \alpha| - \omega^2 \right], \quad (5) \\ &+ \sum_{\alpha=\langle ij \rangle} [k_\alpha - k_{\text{eff}}(\omega)] |\alpha\rangle \langle \alpha|, \\ &\equiv \hat{\mathcal{G}}_{\text{eff}}(\omega)^{-1} + \hat{\mathcal{V}}(\omega), \end{aligned}$$

where $\hat{\mathcal{G}}_{\text{eff}}(\omega) \equiv \hat{\mathcal{G}}_{K=k_{\text{eff}}(\omega)}(\omega)$. By treating the second term $\hat{\mathcal{V}}(\omega)$ as a perturbation, we can write the transfer matrix as

$$\begin{aligned} \hat{\mathcal{T}}(\omega) &= \sum_{\alpha=\langle ij \rangle} \hat{\mathcal{T}}_\alpha(\omega) \\ &+ \sum_{\alpha=\langle ij \rangle} \sum_{\beta \neq \alpha} \hat{\mathcal{T}}_\alpha(\omega) \hat{\mathcal{G}}_{\text{eff}}(\omega) \hat{\mathcal{T}}_\beta(\omega) + \dots \end{aligned} \quad (6)$$

where

$$\hat{\mathcal{T}}_\alpha(\omega) = \frac{k_{\text{eff}}(\omega) - k_\alpha}{1 - [k_{\text{eff}}(\omega) - k_\alpha] \langle \alpha | \hat{\mathcal{G}}_{\text{eff}}(\omega) | \alpha \rangle} |\alpha\rangle \langle \alpha|. \quad (7)$$

The self-consistent equation for the effective stiffness $k_{\text{eff}}(\omega)$ is [40, 41]

$$\frac{k_{\text{eff}}(\omega) - k_\alpha}{1 - [k_{\text{eff}}(\omega) - k_\alpha] \langle \alpha | \hat{\mathcal{G}}_{\text{eff}}(\omega) | \alpha \rangle} = 0. \quad (8)$$

To proceed, we use an identity derived from a trivial relation $\hat{\mathcal{G}}_{\text{eff}}(\omega) (\hat{\mathcal{M}} - \omega^2) = \hat{1}$ [40, 41]:

$$\langle \alpha | \hat{\mathcal{G}}_{\text{eff}}(\omega) | \alpha \rangle = \frac{1}{k_{\text{eff}} d} [1 + \omega^2 G(\omega)], \quad (9)$$

where $G(\omega) \equiv \langle i | \hat{\mathcal{G}}_{\text{eff}}(\omega) | i \rangle$. Thus, we have

$$\frac{k_{\text{eff}}(\omega) - k_\alpha}{1 - [k_{\text{eff}}(\omega) - k_\alpha] \frac{1}{k_{\text{eff}} d} [1 + \omega^2 G(\omega)]} = 0, \quad (10)$$

where

$$G(\omega) = \int_{\mathbf{q} \in [-\pi, \pi]^d} \frac{d\mathbf{q}}{(2\pi)^d} \frac{1}{k_{\text{eff}}(\omega) q^2 - \omega^2}. \quad (11)$$

In the following, we apply the Debye approximation to Eq. (11), in which we represent the cubic first Brillouin zone as a sphere with the same volume, as follows:

$$G(\omega) = \int_{0 < |\mathbf{q}| < q_D} \frac{d\mathbf{q}}{(2\pi)^d} \frac{1}{k_{\text{eff}}(\omega) q^2 - \omega^2}, \quad (12)$$

where the radius of the sphere q_D is determined as follows:

$$1 = \int_{0 < |\mathbf{q}| < q_D} \frac{d\mathbf{q}}{(2\pi)^d} = \frac{q_D^d S_{d-1}}{d(2\pi)^d}. \quad (13)$$

S_{d-1} is the area of a $(d-1)$ -dimensional sphere with radius 1.

Generally, the effective stiffness is a complex number $k_{\text{eff}}(\omega) = k_r(\omega) - i\Sigma(\omega)$, and when the solution has a finite imaginary part at zero frequency, $\Sigma(0) > 0$, the system is unstable. The imaginary part of $G(\omega)$ yields the vDOS

$$g(\omega) = \frac{2\omega}{\pi} \text{Im } G(\omega), \quad (14)$$

To solve Eq. (10) with some specified $P(k_\alpha)$, we transform it into a useful form, as follows:

$$\frac{1}{k_\alpha + \kappa(\omega)} = \frac{1 + \omega^2 G(\omega)}{dk_{\text{eff}}(\omega)}, \quad (15)$$

where

$$\kappa(\omega) \equiv \frac{d-1 - \omega^2 G(\omega)}{1 + \omega^2 G(\omega)} k_{\text{eff}}(\omega). \quad (16)$$

It should be noted that $\kappa(\omega) \rightarrow (d-1)k_{\text{eff}}(0)$ as $\omega \rightarrow 0$. Thus, we can assume $\text{Im } \kappa(\omega) \sim \text{Im } k_{\text{eff}}(\omega) < 0$ as long as we focus on the low-frequency region.

C. Large dimension limit

In this section, we solve Eq. (10) in the large-dimension limit. This is crucial because the EMA becomes exact

as $d \rightarrow \infty$ [53]. We do not assume the specific form of the distribution $P(k_\alpha)$ and only require that its moment-generating function is finite.

As $d \rightarrow \infty$ and $\omega \rightarrow 0$, $G(\omega)$ in Eq. (12) can be approximated as

$$G(\omega) \simeq \frac{1}{k_{\text{eff}}(\omega)q_D^2 - \omega^2}. \quad (17)$$

Its derivation is provided in Appendix A. Using Eq. (17), Eq. (10) becomes

$$\frac{k_{\text{eff}} - k_\alpha}{1 - \frac{k_{\text{eff}}(\omega) - k_\alpha}{d[k_{\text{eff}}(\omega)q_D^2 - \omega^2/q_D^2]}} = 0. \quad (18)$$

The denominator can be expanded as [52]

$$k_{\text{eff}}(\omega) - \overline{k_\alpha} + \frac{1}{d} \frac{[k_{\text{eff}}(\omega) - k_\alpha]^2}{k_{\text{eff}}(\omega) - \omega^2/q_D^2} = 0. \quad (19)$$

Therefore, the self-consistent equation is expressed as follows:

$$k_{\text{eff}}(\omega)^2 - (\mu + \omega^2/q_D^2)k_{\text{eff}}(\omega) + \mu\omega^2/q_D^2 + (\sigma^2 + \mu^2)/d = 0, \quad (20)$$

where σ^2 is the variance of the distribution $P(k_\alpha)$; $\sigma^2 \equiv \overline{(k_\alpha - \mu)^2} = \int dk_\alpha (k_\alpha - \mu)^2 P(k_\alpha)$. Solving this quadratic equation, we obtain two solutions, and the one that satisfies $k_{\text{eff}} = \mu$ at $\sigma = \omega = 0$ is chosen:

$$k_{\text{eff}}(\omega) = \frac{1}{2}(\mu + \omega^2/q_D^2) + \frac{1}{2}\sqrt{\mu^2 - 4\sigma^2/d - 2\mu\omega^2/q_D^2 + \omega^4/q_D^4}. \quad (21)$$

The critical value of the standard deviation σ_c , above which the system is unstable: $\Sigma(0) > 0$, is $\sigma_c = \sqrt{d}\mu/2 \sim d^{1/2}\mu$. Its dependence on dimension is clear to understand as follows. The mean and standard deviation of the sum of all spring constants around an element are of the order $d\mu$ and $d^{1/2}\sigma$, respectively. When they are of the same order, which gives σ_c , the system is destabilized. This instability has been observed in many elasticity models with perturbations [39, 46, 58], and we refer to it as the conventional instability [51].

For $\sigma \leq \sigma_c$, the solution changes its behavior at the frequency

$$\omega_0 \equiv q_D \sqrt{(\mu^2 - 4\sigma^2/d)/2\mu} = \sqrt{\frac{2q_D^2}{d\mu}} \sqrt{\sigma_c^2 - \sigma^2}. \quad (22)$$

Using ω_0 , Eq. (21) can be written as

$$k_{\text{eff}}(\omega) = \frac{1}{2}(\mu + \omega^2/q_D^2) + \sqrt{\frac{\mu}{2}} \sqrt{(\omega_0^2 - \omega^2)/q_D^2 + \omega^4/q_D^4}, \quad (23)$$

At $\omega = \omega_0$, its real part $k_r(\omega) \equiv \text{Re } k_{\text{eff}}(\omega)$ reduces by a numerical factor, which leads to a local minimum in the phase velocity of sound, which is often referred to as sound softening [40]. Because the region of the Rayleigh scattering $\Sigma \sim \omega^d$ vanishes as $d \rightarrow \infty$, the imaginary part $\Sigma(\omega) \equiv -\text{Im } k_{\text{eff}}(\omega)$ is zero at $\omega < \omega_0$ and $\Sigma(\omega) \sim \omega$ at $\omega \gg \omega_0$.

The vDOS is described as

$$g(\omega) = \frac{2\omega}{\pi} \text{Im } G(\omega) \sim \omega\Sigma. \quad (24)$$

Therefore, $g(\omega) \sim \omega^2$ at $\omega \gg \omega_0$, which is referred to as

non-Debye scaling [21, 41, 42]. As $\sigma \rightarrow \sigma_c$, we have $\omega_0 \rightarrow 0$, that is, the gapless non-Debye scaling. It should be noted that in the SDM, the non-Debye scaling is universal among any distribution in the large-dimension limit as long as the distribution $P(k_\alpha)$ has finite moments.

D. Uniform distribution of stiffness

We now focus on specific distributions $P(k_\alpha)$ in finite dimensions under the EMA. It should be noted that the EMA is not only exact as $d \rightarrow \infty$ but also a good approximation in finite d [53]. First, we investigate the model with the uniform distribution

$$P(k_\alpha) = \begin{cases} \frac{1}{2\Delta} & k_\alpha \in [\mu - \Delta, \mu + \Delta] \\ 0 & \text{otherwise} \end{cases}. \quad (25)$$

The variance is $\sigma^2 = \Delta^2/3$. This model provides essentially the same results as those in the large-dimension limit. The self-consistent equation with a uniform distribution is easy to solve and has been used in previous studies [52, 58]. Although our analysis is almost equivalent to the previous works, this model is a useful example for the following discussion. Therefore, we present the results for completeness.

By averaging Eq. (15) over k_α , we obtain

$$\begin{aligned} \frac{\mu + \kappa(\omega)}{\Delta} &= \coth \left\{ \frac{\Delta}{dk_{\text{eff}}(\omega)} [1 + \omega^2 G(\omega)] \right\}, \\ &\simeq \frac{dk_{\text{eff}}(\omega)}{\Delta [1 + \omega^2 G(\omega)]} + \frac{1}{3} \frac{\Delta}{dk_{\text{eff}}(\omega)} [1 + \omega^2 G(\omega)]. \end{aligned} \quad (26)$$

In the second line, we use a series expansion of \coth , which is justified by $\Delta/d\mu \ll 1$. Using the definition of $\kappa(\omega)$ in Eq. (16), the equation is simplified to

$$k_{\text{eff}}(\omega)^2 - \mu k_{\text{eff}}(\omega) + \frac{\sigma^2}{d} + \frac{\sigma^2}{d} \omega^2 G(\omega) = 0. \quad (27)$$

We focus on the lowest-frequency region and approximate Green's function of Eq. (12) as follows:

$$\begin{aligned} G(\omega) &\simeq \frac{1}{k_{\text{eff}}(\omega)} \int_{0 < |q| < q_D} \frac{d\mathbf{q}}{(2\pi)^d} \frac{1}{\mathbf{q}^2}, \\ &= \frac{S_{d-1}}{k_{\text{eff}}(\omega)(2\pi)^d} \int_0^{q_D} dq q^{d-3}, \\ &= \frac{1}{k_{\text{eff}}(\omega)} \frac{d}{(d-2)q_D^2} \equiv \frac{A_d}{k_{\text{eff}}(\omega)}, \end{aligned} \quad (28)$$

where we obtain the third line from the second using Eq. (13). Therefore, Eq. (27) reduces to

$$k_{\text{eff}}(\omega)^3 - \mu k_{\text{eff}}(\omega)^2 + \frac{\sigma^2}{d} k_{\text{eff}}(\omega) + \frac{\sigma^2}{d} A_d \omega^2 = 0. \quad (29)$$

At zero frequency, this equation is the same as Eq. (20), and $\sigma = \sigma_c \equiv \sqrt{d}\mu/2$ is the critical point for stability. When $\omega \neq 0$, we approximate the equation under the condition $(\sigma_c^2 - \sigma^2)/d\mu^2 \sim \omega^2/\mu \ll 1$ in Appendix B, which yields the solution

$$k_{\text{eff}}(\omega) = \frac{\mu}{2} - i\sqrt{\frac{\mu}{2}} \sqrt{A_d \omega^2 - A_d \omega_0'^2}. \quad (30)$$

where

$$\omega_0' \equiv \sqrt{\frac{2}{d\mu A_d}} \sqrt{\sigma_c^2 - \sigma^2}. \quad (31)$$

It should be noted that $A_d \rightarrow q_D^{-2}$ and $\omega_0' \rightarrow \omega_0$ as $d \rightarrow \infty$. This is consistent with Eq. (23). It is essential to mention that in the case of a uniform distribution, the solution in the large-dimension limit is a good approximation, even in finite dimensions. The SDM with a uniform distribution is destabilized by the conventional instability.

E. Gaussian distribution of stiffness

Next, we consider a Gaussian distribution with a mean of μ and variance of σ^2 . This seems to be natural for coarse-grained stiffness [38, 57]. The Gaussian distribution produces results that are qualitatively different from those of the uniform distribution. We will notice that the results of the Gaussian distribution are key to understanding the mechanism behind the stability of the system within the framework of the EMA.

By averaging Eq. (15) with the Gaussian distribution, we obtain

$$\frac{1}{\sqrt{2\pi}} \int_{-\infty}^{\infty} dx \frac{e^{-x^2}}{x+z} = \frac{\sigma}{dk_{\text{eff}}(\omega)} [1 + \omega^2 G(\omega)], \quad (32)$$

where we use the condition $\text{Im} \kappa(\omega) < 0$, and $z = [\mu + \kappa(\omega)]/\sqrt{2}\sigma^2$. The left-hand side is further calculated as

$$\frac{1}{\sqrt{2\pi}} \int_{-\infty}^{\infty} dx \frac{e^{-x^2}}{x+z} = \sqrt{2} e^{-z^2} \int_0^z dl e^{l^2} + i\sqrt{\frac{\pi}{2}} e^{-z^2}. \quad (33)$$

Therefore, the self-consistent equation is expressed as

$$F(z) + i\frac{\sqrt{\pi}}{2} e^{-z^2} = \frac{\sigma}{\sqrt{2}dk_{\text{eff}}(\omega)} [1 + \omega^2 G(\omega)], \quad (34)$$

where $F(z)$ is the Dawson function.

1. Zero-frequency limit

It is instructive to discuss the zero-frequency limit. In this case, Eq. (34) becomes

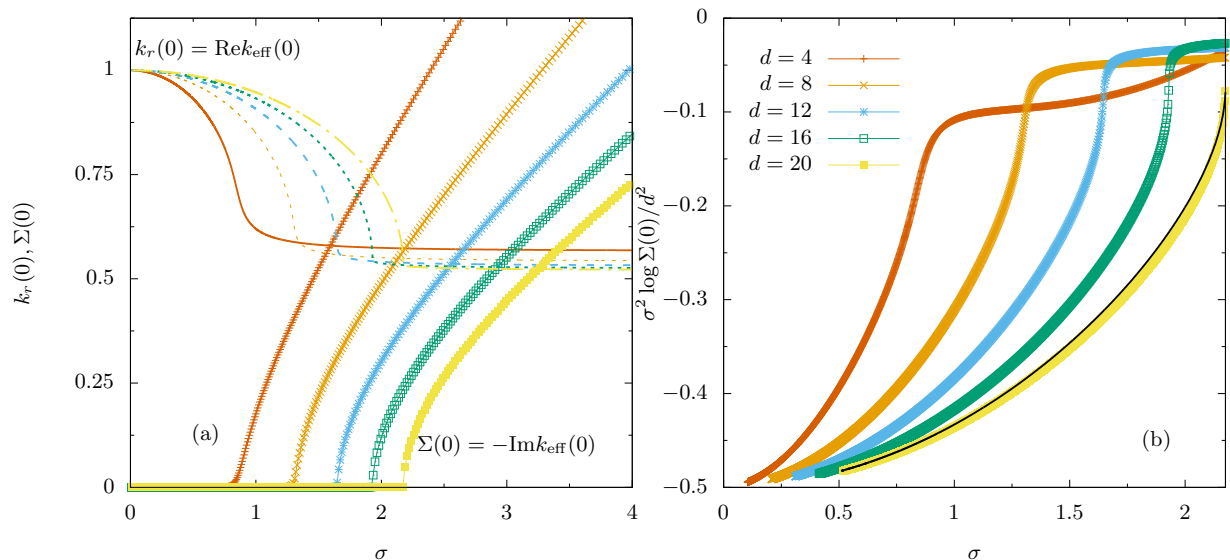


FIG. 1. (a) Real and imaginary parts of effective stiffness for model with Gaussian distribution as functions of σ at zero frequency. We change spatial dimension from $d = 4$ to $d = 20$. (b) $\sigma^2 \log \Sigma(0) / d^2$ vs σ . Solid line represents approximate form in Eq. (37).

$$F \left[\frac{\mu + (d-1)k_{\text{eff}}(0)}{\sqrt{2\sigma^2}} \right] + i \frac{\sqrt{\pi}}{2} \exp \left\{ - \left[\frac{\mu + (d-1)k_{\text{eff}}(0)}{\sqrt{2\sigma^2}} \right]^2 \right\} = \frac{\sigma}{\sqrt{2}dk_{\text{eff}}(0)}. \quad (35)$$

Remarkably, if the imaginary part of $k_{\text{eff}}(0)$ is zero (or infinitesimally small), the equation does not hold because of the second term on the left-hand side. That is, we cannot have a stable solution at any σ for the Gaussian distribution. This is somewhat counter-intuitive, and we discuss its meaning briefly in the following.

As we described in Section II C, we can obtain a stable solution at $\sigma < \sigma_c = \sqrt{d}\mu/2$ in the large-dimension limit. Here, we describe how the solution for the Gaussian distribution converges to Eq. (21) as $d \rightarrow \infty$. Because the calculation is straightforward but tedious, we present it in Appendix C and only present the results here. As $d \rightarrow \infty$, the real part is

$$k_r(0) = \frac{\mu}{2} + \frac{1}{2} \sqrt{\mu^2 - 4 \frac{\sigma^2}{d}} \quad (36)$$

and the imaginary part is

$$\Sigma(0) = \sqrt{\frac{\pi}{2}} \frac{d^2 k_r(0)^4 \exp \left[-\frac{d^2 k_r(0)^2}{2\sigma^2} \right]}{\mu \sigma \left[k_r(0) - 2 \frac{\sigma^2}{\mu d} \right]}. \quad (37)$$

When we set $\sigma = \sqrt{d}(\mu - \epsilon)/2$ with $0 < \epsilon \ll 1$, the real part becomes $k_r(0) = \mu/2 + \sqrt{2\mu\epsilon}$. Therefore, the imaginary part is expressed as

$$\Sigma(0) \simeq \frac{\sqrt{\pi}}{16} \frac{d^{3/2} \mu^2}{\sqrt{\mu\epsilon}} e^{-d/2} \sim d^{3/2} e^{-d/2} \epsilon^{-1/2}. \quad (38)$$

This is exponentially small when $\sigma \ll \sqrt{d}\mu$ and asymptotically vanishes as $d \rightarrow \infty$. Therefore, as $d \rightarrow \infty$, the solutions converge to Eq. (21). The imaginary part grows rapidly when σ approaches the critical value $\sigma_c \equiv \sqrt{d}\mu/2$ and exhibits singular behavior $\Sigma(0) \sim \epsilon^{-1/2}$, which is a crossover in finite dimensions and becomes a transition in the large-dimension limit.

We also numerically solved Eq. (35), and the results are presented in Fig. 1. Figure 1(a) presents the plots of the effective stiffness as functions of the standard deviation in $d = 4, 8, 12, 16$, and 20 . Figure 1(b) depicts $\sigma^2 \log \Sigma(0) / d^2$. From Eq. (37), $\sigma^2 \log \Sigma(0) / d^2 \rightarrow -1/2$ as $\sigma \rightarrow 0$, regardless of d . Equation (37) is also represented by the solid line.

2. Finite frequency

In the case of finite frequency, we solve Eq. (34) numerically and present the results in Fig. 2. Figure 2(a) depicts the real parts of the effective stiffness $k_r(\omega) = \text{Re}k_{\text{eff}}(\omega)$ for $\sigma = 0.6, 0.65, 0.7$, and 0.75 and $d = 3$. They become smaller at approximately $\omega = 1$ than those at $\omega = 0$, except for the case of $\sigma = 0.75$. These local minima are also described in Section II C and correspond to the local minimum of the sound velocity. In the case of $\sigma = 0.75$, the system is unstable even in the sense of conventional instability. When we further increase

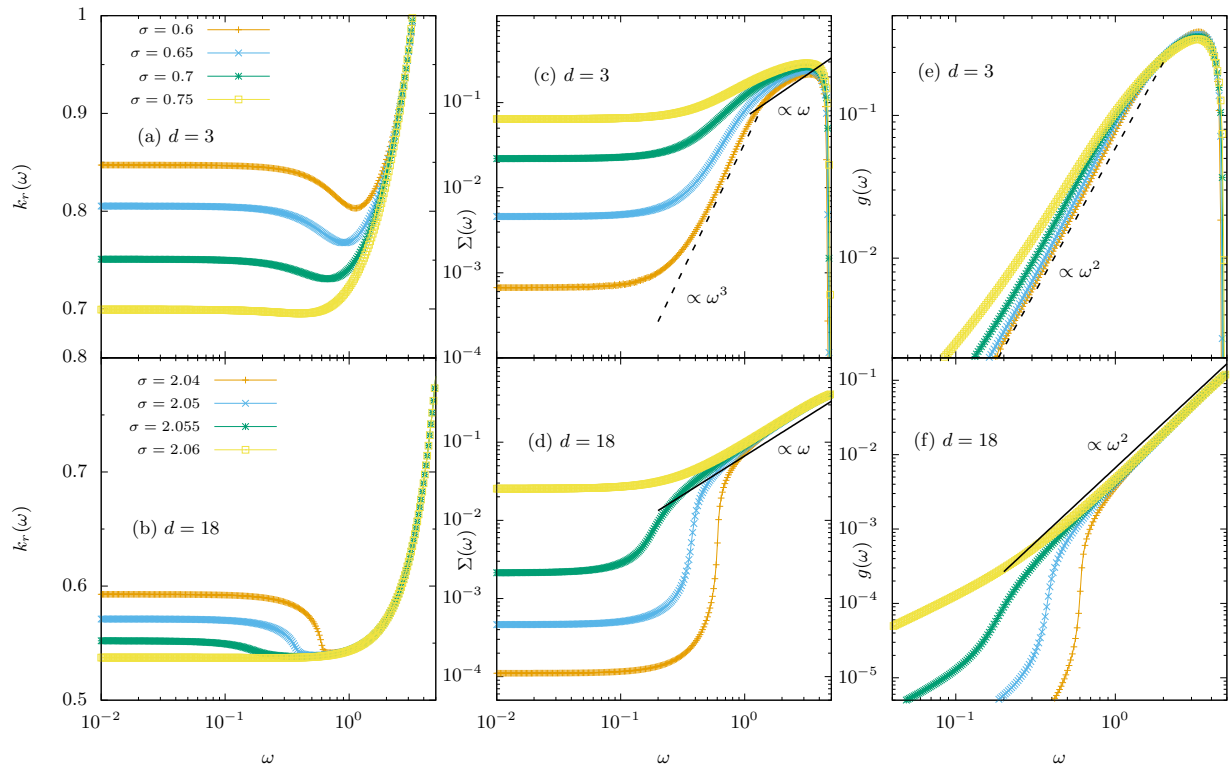


FIG. 2. (a) Real parts of effective stiffness as functions of frequency for some σ in $d = 3$. (b) Same plot as panel (a) in $d = 18$. (c) Imaginary parts of effective stiffness as functions of frequency in $d = 3$. Values of σ are same as in panel (a). Solid line is proportional to ω , and dashed line is proportional to $\omega^d = \omega^3$. (d) Same plot as panel (c) in $d = 18$. Values of σ are same as in panel (b). (e) vDOS in $d = 3$ for same values of σ as in panel (a). Tail of vDOS represents $g(\omega) \sim \omega^2$ (dashed line), which is Debye scaling of phonons. (f) Same plot as in panel (e) in $d = 18$ for same values of σ as in panel (b). Debye scaling $\omega^{d-1} = \omega^{17}$ is practically impossible to observe, whereas non-Debye scaling $g(\omega) \sim \omega^2$ (solid line) grows compared to $d = 3$ case.

the frequency, all the real parts increase, but remain of the order of one. Figure 2(b) presents the equivalent results for $d = 18$ and $\sigma = 2.04, 2.05, 2.065$, and 2.06 . The qualitative behavior is the same as that depicted in Fig. 2(a), and the data for $\sigma = 2.06$ correspond to those for $\sigma = 0.75$ for $d = 3$.

Figure 2(c) depicts the imaginary parts $\Sigma(\omega) = -\text{Im} k_{\text{eff}}(\omega)$ for $d = 3$ and the same value of σ . In the lowest-frequency region, they converge to zero-frequency-limit values. When we increase the frequency, we obtain the scaling $\Sigma(\omega) \sim \omega^d$, which is characteristic of Rayleigh scattering [40, 41]. This scaling is clear for the smallest value of σ , but is smeared when σ is increased. In the highest-frequency region, we can see the non-Debye scaling $\Sigma(\omega) \sim \omega$. Figure 2(d) is the equivalent plot for $d = 18$ for the same value of σ as depicted in Fig. 2(b). It is practically difficult to observe the contribution from the Rayleigh scattering $\Sigma(\omega) \sim \omega^d$; instead, the non-Debye scaling $\Sigma(\omega) \sim \omega$ region grows significantly compared to that depicted in Fig 2(c).

Figures 2(e) and (f) depict the corresponding vDOS for $d = 3$ and $= 18$, respectively. Although the same frequency dependence $g(\omega) \sim \omega^2$ is evident in both the

plots, their meanings are different from each other. In Fig. 2(c), it is the Debye scaling of phonons $g_{\text{Debye}}(\omega) \sim \omega^{d-1}$, whereas in Fig. 2(d), it is the non-Debye scaling, which implies quadratic frequency dependence regardless of d . The ranges of the non-Debye scaling for $d = 3$ and the Debye scaling for $d = 18$ are too narrow to observe. It should be noted that the linear frequency dependence in the lowest-frequency region, which is particularly evident in Fig. 2(f), is simply caused by the plateau of the zero-frequency value of $\Sigma(\omega)$.

F. Restrictions on probability distribution

1. Local instability

In this section, we consider, from general arguments, why the Gaussian distribution cannot provide a stable solution. We will introduce another mechanism of instability, which we refer to as the “local instability” The argument is the same as in the preceding paper [51], but it should be easier to understand with the examples provided in the preceding sections.

Because we are interested only in the stability of the system, it is enough to consider the zero-frequency limit. Thus, we consider the self-consistent equation in the zero-frequency limit as

$$\int \frac{dk_\alpha P(k_\alpha)}{k_\alpha + (d-1)k_{\text{eff}}(0)} = \frac{1}{dk_{\text{eff}}(0)}. \quad (39)$$

Suppose that the solution has only an infinitesimally small imaginary part, that is, $k_{\text{eff}}(0) - i\epsilon$ with $\epsilon \ll 1$. Therefore, the left-hand side of the equation becomes

$$\mathcal{P} \int \frac{dk_\alpha P(k_\alpha)}{k_\alpha + (d-1)k_{\text{eff}}(0)} + i\pi P[-(d-1)k_{\text{eff}}(0)], \quad (40)$$

where \mathcal{P} indicates the Cauchy principal value. Therefore, the condition

$$P[-(d-1)k_{\text{eff}}(0)] = 0. \quad (41)$$

is necessary for the solution to be real. Conversely, if this condition is violated, the system is unstable, with the emergence of the imaginary part, $\Sigma(0) > 0$. This is the origin of local instability. This readily leads to the fact that all distributions supported on the whole real line \mathbb{R} , for example, the Gaussian distribution, cannot yield a stable solution.

2. Interpretation of local instability using defect model

To illustrate a simple physical interpretation of the local instability, we consider a defect model. In this model, all springs have the same stiffness $k_{\text{eff}}(0) > 0$ except for a defect with stiffness k_α .

The dynamical matrix of the defect model is as follows:

$$\hat{\mathcal{M}}_d = k_{\text{eff}}(0) \sum_{\beta=\langle kl \rangle} |\beta\rangle \langle \beta| + [k_\alpha - k_{\text{eff}}(0)] |\alpha\rangle \langle \alpha|. \quad (42)$$

Upon calculating the transfer matrix for this dynamical matrix, one can see that only the first term of the expansion in Eq. (6) remains, and the total Green's function is expressed as

$$\hat{\mathcal{G}}_d(\omega) = \hat{\mathcal{G}}_0(\omega) + \hat{\mathcal{G}}_0(\omega) \hat{\mathcal{T}}_{\alpha 0}(\omega) \hat{\mathcal{G}}_0(\omega), \quad (43)$$

where $\hat{\mathcal{G}}_0(\omega) = \hat{\mathcal{G}}_{K=k_{\text{eff}}(0)}(\omega)$, and $\hat{\mathcal{T}}_{\alpha 0}(\omega)$ is expressed by Eq. (7) with $k_{\text{eff}}(\omega) \rightarrow k_{\text{eff}}(0)$ and $\hat{\mathcal{G}}_{\text{eff}}(\omega) \rightarrow \hat{\mathcal{G}}_0(\omega)$, that is,

$$\hat{\mathcal{T}}_{\alpha 0}(\omega) = \frac{k_{\text{eff}}(0) - k_\alpha}{1 - [k_{\text{eff}}(0) - k_\alpha] \langle \alpha | \hat{\mathcal{G}}_0(\omega) | \alpha \rangle} |\alpha\rangle \langle \alpha|. \quad (44)$$

From Eq. (44), we see that $\hat{\mathcal{T}}_{\alpha 0}(\omega)$ diverges when $k_\alpha = -(d-1)k_{\text{eff}}(0)$, which means that the system has a non-trivial zero mode.

This zero mode can be constructed as (without normalization):

$$|0\rangle \equiv \hat{\mathcal{G}}_0(0) |\alpha\rangle. \quad (45)$$

The eigenrelation $\hat{\mathcal{M}}|0\rangle = 0$ can be checked as follows: The product of the first term in Eq. (42) and $|0\rangle$ yields $|\alpha\rangle$. The second term yields

$$\begin{aligned} & [k_\alpha - k_{\text{eff}}(0)] |\alpha\rangle \langle \alpha | 0 \rangle, \\ & = [k_\alpha - k_{\text{eff}}(0)] |\alpha\rangle \langle \alpha | \hat{\mathcal{G}}_0(0) | \alpha \rangle \\ & = \frac{\theta}{k_{\text{eff}}} [k_\alpha - k_{\text{eff}}(0)] |\alpha\rangle, \end{aligned} \quad (46)$$

where we use Eq. (9). Therefore, we obtain

$$\hat{\mathcal{M}}|0\rangle = \left\{ 1 + \frac{\theta[k_\alpha - k_{\text{eff}}(0)]}{k_{\text{eff}}(0)} \right\} |\alpha\rangle \quad (47)$$

Therefore, $\hat{\mathcal{M}}|0\rangle = 0$ when the ‘‘defect’’ bond α has a negative stiffness $k_\alpha = -(d-1)k_{\text{eff}}(0)$.

When $k_\alpha < -(d-1)k_{\text{eff}}(0)$, the system is unstable along the direction $|0\rangle$. This provides an interpretation of the stability condition Eq. (41) as follows. When Eq. (41) is violated, a number of springs become ‘‘defects’’ and produce unstable modes. We emphasize that the instability identified here is different from the conventional instability described in the preceding section. We thus conclude that the singular behavior of the solution for the Gaussian distribution (see Eq. (38)) can be interpreted as a transition from the local instability to the conventional instability.

We argue that the unstable modes associated with the local instability have a strong similarity with the QLVs, as described in the following. First, the mode $|0\rangle$ is the response to a local dipolar force in an unperturbed homogeneous system. The elasticity theory illustrates that this response field has an asymptotic spatial profile $\propto r^{2(1-d)}$, where r is the distance to the force, and the QLVs have the same profile far from the core [24, 29]. Second, the response to the dipolar force in glasses has a core whose size is the same as that of the QLVs [28, 30]. Third, the energetics of the QLVs are equivalent to $|0\rangle$; the unstable core corresponds to the second term in Eq. (47), whereas the stable far-field components correspond to the first term in Eq. (47).

3. Restrictions on tail to avoid local instability

Generally, we do not know which instability is caused by a particular distribution, but we can derive a sufficient condition to avoid the local instability. We consider the distribution supported on a finite interval $[-k_{\text{min}}, k_{\text{max}}]$ with $k_{\text{min}}, k_{\text{max}} > 0$. Suppose we have the critical real solution $k_{\text{eff}}(0) = k_{\text{min}}/(d-1)$ in the sense of the local instability, that is,

$$\int_{-k_{\text{min}}}^{k_{\text{max}}} \frac{dk_\alpha P(k_\alpha)}{k_\alpha + k_{\text{min}}} = \frac{d-1}{dk_{\text{min}}}. \quad (48)$$

Based on the frequency dependence of the critical solution, we can derive the condition. Because we consider only the lowest-frequency region, we use Eq. (28)

for Green's function. To solve Eq. (15), we further approximate $\kappa(\omega)$ as

$$\kappa(\omega) = (d-1)k_r(\omega) - dA_d\omega^2 - i(d-1)\Sigma(\omega), \quad (49)$$

and assume that $\text{Re}[\kappa(\omega)] \gg \text{Im}[\kappa(\omega)]$. Thus, the self-consistent equation for the real part is

$$\mathcal{P} \int_{-k_{\min}}^{k_{\max}} \frac{dk_{\alpha} P(k_{\alpha})}{k_{\alpha} + (d-1)k_r(\omega) - dA_d\omega^2} = \frac{1}{dk_r(\omega)} \left[1 + \frac{A_d\omega^2}{k_r(\omega)} \right]. \quad (50)$$

Subtracting Eq. (48) from Eq. (50), we obtain

$$\mathcal{P} \int_{-k_{\min}}^{k_{\max}} \frac{dk_{\alpha} P(k_{\alpha})}{[k_{\alpha} + k_{\min} + \delta k_r(\omega) - dA_d\omega^2] (k_{\alpha} + k_{\min})} = \frac{d-1}{d[k_{\min} + \delta k_r(\omega)]} \frac{-\frac{\delta k_r(\omega)}{k_{\min}} + \frac{A_d\omega^2}{k_{\min} + \delta k_r(\omega)}}{-\delta k_r(\omega) + dA_d\omega^2} \quad (51)$$

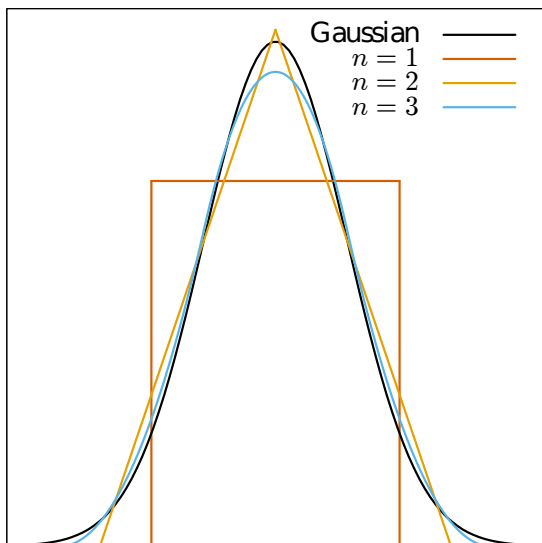


FIG. 3. Gaussian and Bates distributions ($n = 1, 2$, and 3) with same mean and standard deviation.

where we decompose the real part of the solution as $k_r(\omega) = [k_{\min} + \delta k_r(\omega)] / (d-1)$. Because we expect $\delta k_r(\omega) < 0$ for consistency with the results in the preceding sections, $-\delta k_r(\omega) + dA_d\omega^2 \neq 0$ for $\omega \neq 0$. Therefore, if the distribution behaves as $P(k_{\alpha}) \sim (k_{\alpha} + k_{\min})^{\nu}$ with $\nu \leq 1$ at $k_{\alpha} \simeq -k_{\min}$, the left-hand side diverges as ω moves toward zero frequency, whereas the right-hand side is always finite regardless of the frequency dependence of $\delta k_r(\omega)$. Hence, when the distribution decays with a power $\nu \leq 1$ near its lower cutoff, it avoids the local instability. Conversely, when $\nu > 1$, we cannot exclude the possibility of local instability. This condition is used in Section II H.

G. Bates distribution of stiffness

In the preceding Sections II E and II F, it has been established that the Gaussian distribution always induces

local instability, and it is not suitable as the stiffness distribution of a stable system. Indeed, this fact is easily acceptable once we recognize that the Gaussian distribution has a finite probability of arbitrarily large negative values. Even if the distribution in the stable system resembles a Gaussian distribution around the mean value, its tail does not continue infinitely and should be cut off at some finite value.

A significant question is which instability generally occurs depending on the stiffness distribution. To obtain an answer this question, we employ the Bates distribution, which is a distribution of the average of n statistically independent uniformly distributed random variables in the interval $[\mu - \Delta, \mu + \Delta]$. The mean is $\mu > 0$ and the variance is $\sigma^2 = \Delta^2/3n$. It includes the uniform ($n = 1$), triangular ($n = 2$), and Gaussian ($n, \Delta \rightarrow \infty$ and $\sigma = \text{const.}$) distributions. See Fig. 3. Because the Gaussian (uniform) distribution always causes local (conventional) instability, the question can be rephrased as follows: "Which instability occurs at general n and Δ ?"

To judge the stability of the model, it suffices to calculate the effective stiffness at zero frequency $k_{\text{eff}}(0)$. Figure 4 presents the numerical results for $d = 3$. Figure 4(a) presents the zero-frequency effective stiffness as a function of the standard deviation σ for $n = 1, 2, 3, 4, 5$, and ∞ of the Bates distributions. The behaviors of the real parts $k_r(0) \equiv \text{Re}[k_{\text{eff}}(0)]$ are qualitatively the same as in the preceding sections for all n . When we increase σ , the imaginary part $\Sigma(0) \equiv -\text{Im}[k_{\text{eff}}(0)]$ starts to be nonzero at some point $\sigma = \sigma_0$ [59] for finite n , whereas the model with the Gaussian distribution $n = \infty$ is always unstable. If it is caused by local instability, Eq. (41) is violated above $\sigma = \sigma_0$. Indeed, we found that the models with $n = 4$ and 5 are destabilized by the local instability, and the instability points are represented by arrows in the figure. We also represent the instability point in the Gaussian case, that is, $\sigma_0 = 0$.

On the other hand, for small $n = 1, 2, 3$, the models seem to illustrate semicircle dependence owing to the conventional instability. Moreover, when we increase σ , we expect a crossover from the local instability to the

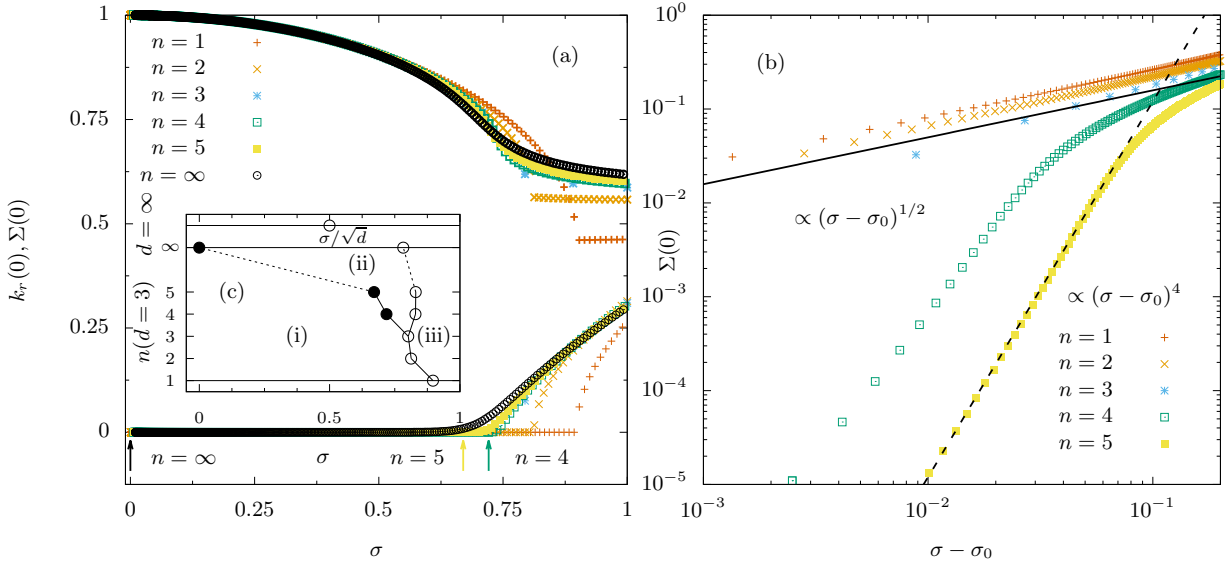


FIG. 4. (a) Real and imaginary parts of effective stiffness for Bates distribution as functions of σ at zero frequency. Arrows for $n = 4, 5$ and ∞ represent the critical values above which system is destabilized by local instability. System with $n \leq 3$ is destabilized by conventional instability. (b) Logarithmic plot of imaginary parts around critical values $\sigma = \sigma_0$. Solid line represents dependence of $\Sigma(0) \sim (\sigma - \sigma_0)^{1/2}$. Dashed line represents dependence of $\Sigma(0) \sim (\sigma - \sigma_0)^4$. (c) Phase diagram for (n, σ) plane in $d = 3$. Open circles represent σ_{fit} (see text for definition), and closed circles represent values above which local instability occurs. Solid and dotted lines represent eye guidance. Plane is divided into three phases: (i) stable phase, (ii) unstable phase owing to local instability, and (iii) unstable phase owing to conventional instability. Above phase diagram in $d = 3$, we present phase diagram in $d = \infty$ represented by solid line. Line is divided into two phases: (i) stable phase at $\sigma/\sqrt{d} < \sigma_c/\sqrt{d} = \mu/2$ and (ii) unstable phase owing to conventional instability at $\sigma/\sqrt{d} > \sigma_c/\sqrt{d}$.

conventional instability even for $n = 4$ and 5 , as in the case of the Gaussian distribution (see Section II E). Essentially, in the region of the largest standard deviation, the imaginary parts for different n almost collapse onto the same semicircle.

In addition, we present the logarithmic plot of the imaginary parts around $\sigma = \sigma_0$ in Fig. 4(b). In the figure, we represent, for guiding the eye, the dependence of $\Sigma(0) \sim (\sigma - \sigma_0)^{1/2}$ using a solid line and that of $\Sigma(0) \sim (\sigma - \sigma_0)^4$ using a dashed line. For $n \leq 3$, the data are fitted well to $\Sigma(0) \sim (\sigma - \sigma_0)^{1/2}$, but for $n \geq 4$, the dependence on σ clearly differs so that $\Sigma(0) \sim (\sigma - \sigma_0)^4$ works well instead. Furthermore, we tried to fit our numerical solutions using the semicircle dependence of $\Sigma(0) = A\sqrt{\sigma^2 - \sigma_{\text{fit}}^2}$ with two fitting parameters A and σ_{fit} (data not provided). It should be noted that we fitted the regions far from σ_0 for $n = 4, 5$ and ∞ to avoid the effects of local instability. For $n = 1, 2$, and 3 , a very good fit is obtained, and $\sigma_{\text{fit}} \simeq \sigma_0$. For larger n , a good fit is obtained only for large σ , and $\sigma_{\text{fit}} (> \sigma_0)$ should be interpreted as the estimate of the crossover point from the local instability to the conventional instability.

Finally, Fig. 4(c) summarizes the critical and crossover points in for $d = 3$ and $d = \infty$. For $d = 3$, the open symbols represent σ_{fit} , which is determined by fitting, and the closed symbols are σ_0 for $n \geq 4$. These values allow us to draw the phase diagram in the (n, σ) plane.

The plane is divided into three phases: (i) the stable phase, (ii) unstable phase owing to local instability, and (iii) unstable phase owing to conventional instability. On the other hand, for $d = \infty$, the phase diagram is quite simple: (i) the stable phase at $\sigma/\sqrt{d} < \sigma_c/\sqrt{d} = \mu/2$ and (ii) the unstable phase owing to the conventional instability at $\sigma/\sqrt{d} > \sigma_c/\sqrt{d}$.

H. Marginal solution by local instability

In the preceding section, we found that the distributions supported in the finite interval $[-k_{\text{min}}, k_{\text{max}}]$ can exhibit local instability. A significant issue is the frequency dependence of the solution when the system is marginally stable owing to local instability.

To address this issue, we focus on the lowest-frequency region at the critical standard deviation, that is, $k_{\text{eff}}(0) = k_{\text{min}}/(d - 1)$. We decompose the real part of the solution $k_r(\omega) \equiv \text{Re} k_{\text{eff}}(\omega) = [k_{\text{min}} + \delta k_r(\omega)]/(d - 1)$ (see Section II F). We also approximate Green's function using Eq. (28) [46]. Thus, the equation for $k_r(\omega)$ is Eq. (50). After solving Eq. (50), the imaginary part $\Sigma(\omega) \equiv -\text{Im} k_{\text{eff}}(\omega)$ is obtained as

$$\Sigma(\omega) = \pi d k_r(\omega)^2 P [-(d - 1)k_r(\omega) + dA_d \omega^2]. \quad (52)$$

We solve Eq. (50) under the conditions $k_{\text{eff}}(0) = k_{\text{min}}/(d - 1)$ and $P(k_\alpha) \sim (k_\alpha + k_{\text{min}})^\nu$ with $\nu > 1$ at

$k_\alpha \sim -k_{\min}$ in Appendix D. The result is

$$\frac{\delta k_r(\omega)}{d-1} = -\frac{dI_2 - dI_1^2}{dI_1^2 - (d-1)I_2} A_d \omega^2 \quad (53)$$

with

$$I_m \equiv \int_{-1}^1 dx \frac{\Delta P(\Delta x + \mu)}{(x+1)^m}, \quad (54)$$

where $k_{\min} = \Delta - \mu$ and $k_{\max} = \Delta + \mu$, as in Sections II D and II G. However, our argument in this section is not restricted to the Bates distribution. Because its numerator is always non-negative, an inequality

$$d < \frac{I_2}{I_2 - I_1^2} \equiv d_t, \quad (55)$$

holds for $\delta k_r(\omega)$ to be negative, which is required for the local minimum of the sound velocity [40, 41].

Finally, when we substitute the real part of the solution $\delta k_r(\omega)$ into Eq. (52), we obtain

$$\Sigma(\omega) \sim \omega^{2\nu}. \quad (56)$$

Its contribution to the vDOS is the following:

$$g_{\text{local}}(\omega) \sim \omega^{2\nu+1}. \quad (57)$$

which is clearly different from the Debye behavior $g_{\text{Debye}}(\omega) \sim \omega^{d-1}$. In the preceding paper [51], we present a model that establishes the quartic law $g_{\text{local}}(\omega) \sim \omega^4$, which is the special case of $\nu = 3/2$ in Eq. (57).

III. VECTOR DISPLACEMENT MODEL

A. Model

Until now, we have focused on the SDM. It is very simple to treat analytically and is enough to qualitatively discuss the vibrations of glasses. However, we can treat a slightly realistic model with vector displacements $\{\mathbf{u}_i\}_{i=1}^N$. We refer to this as the VDM to emphasize that it is different from the SDM.

The equation of motion of the VDM is as follows:

$$\frac{d^2}{dt^2} \mathbf{u}_i = - \sum_{\langle ij \rangle} k_{ij} \mathbf{n}_{ij} \mathbf{n}_{ij} \cdot (\mathbf{u}_i - \mathbf{u}_j), \quad (58)$$

where \mathbf{n}_{ij} is the unit vector from the i th element to the j th element. In the bra-ket notation,

$$\frac{d^2}{dt^2} |u\rangle = -\hat{\mathcal{M}} |u\rangle, \quad (59)$$

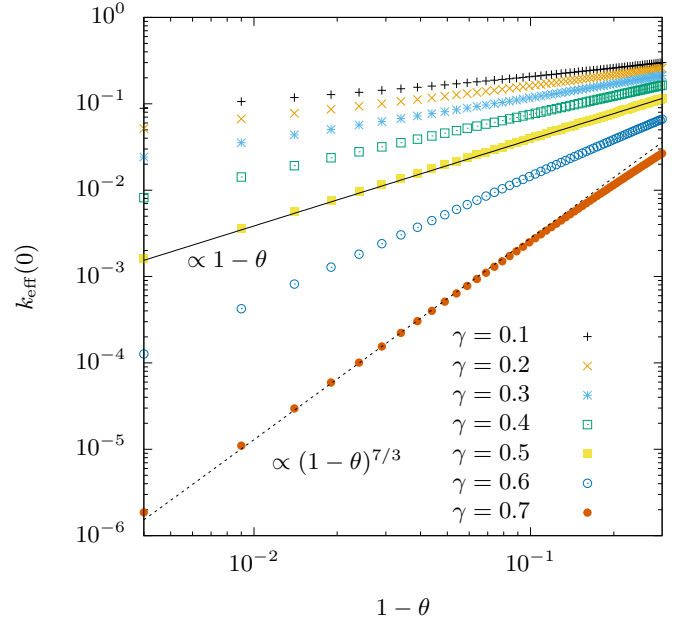


FIG. 5. Effective stiffness at zero frequency for model with Eq. (68). Solid line is proportional to $1 - \theta$ and dotted line is proportional to $(1 - \theta)^{7/3}$, both of which are predicted in Eq. (71).

where

$$\begin{aligned} \hat{\mathcal{M}} &= \sum_{\langle ij \rangle} k_{ij} (|i\rangle - |j\rangle) \mathbf{n}_{ij} \mathbf{n}_{ij}^T (|i\rangle - |j\rangle), \\ &\equiv \sum_{\alpha=\langle ij \rangle} k_\alpha |\alpha\rangle \mathbf{n}_\alpha \mathbf{n}_\alpha^T \langle \alpha|. \end{aligned} \quad (60)$$

It should be noted that for the VDM, we cannot choose a simple cubic lattice because it does not have a finite shear modulus. Specifically, we need a lattice whose coordination number z must be greater than the Maxwell criterion $2d$, below which the network loses rigidity.

The Green's function for the VDM differs because of the choice of the lattice, but we expect that low-frequency properties are universal and do not depend on the lattice. Thus, we consider the simplified Green's function for a homogeneous system:

$$\begin{aligned} \hat{G}_K(\mathbf{r}_{ij}, \omega) &\equiv \langle i | \hat{\mathcal{G}}_K(\omega) | j \rangle \\ &= \int_0^{qD} \frac{d\mathbf{q}}{(2\pi)^d} \frac{e^{i\mathbf{q} \cdot \mathbf{r}_{ij}}}{K\mathbf{q}^2 - \omega^2} \hat{\delta}_d, \end{aligned} \quad (61)$$

where $\hat{\delta}_d$ is the $d \times d$ identity matrix [40, 41, 45, 46]. This is the same as Green's function for the SDM except for the factor $\hat{\delta}_d$.

As in the case of the SDM, we obtain the self-consistent equation for the VDM as

$$\frac{k_{\text{eff}}(\omega) - k_\alpha}{1 - [k_{\text{eff}}(\omega) - k_\alpha] \frac{\theta}{k_{\text{eff}}(\omega)} [1 + \omega^2 G(\omega)]} = 0, \quad (62)$$

where

$$G(\omega) = \frac{1}{d} \text{Tr} \hat{G}_{\text{eff}}(\mathbf{0}, \omega) = \int_0^{q_D} \frac{d\mathbf{q}}{(2\pi)^d} \frac{1}{k_{\text{eff}}(\omega) \mathbf{q}^2 - \omega^2}, \quad (63)$$

and $\theta = 2n_{\text{dof}}/z$. n_{dof} is the number of degrees of freedom per element and $n_{\text{dof}} = d$ in the VDM. For the SDM in the simple cubic lattice, $z = 2d$ and $n_{\text{dof}} = 1$; thus, $\theta = 1/d$. Essentially, when we replace θ by $1/d$, we reproduce Eq. (10).

B. Difference from SDM

Because the self-consistent equations for the VDM and the SDM are almost the same, we refrain from repeating the entire analysis of the SDM. In this section, we explain how the results for the SDM are modified for the VDM. In the case of the zero-frequency limit, we can obtain the results for the VDM by replacing d in the results of the SDM by $1/\theta$. For example, Eq. (41) is modified as follows:

$$P[-(\theta - 1)k_{\text{eff}}(0)/\theta] = 0, \quad (64)$$

which was already reported in the preceding paper [51]. In the case of finite frequency, we need to replace d with θ , except for A_d defined in Eq. (28). Therefore, Eq. (53) is modified as follows:

$$\frac{\delta k_r(\omega)}{\theta^{-1} - 1} = -\frac{I_2 - I_1^2}{I_1^2 - (1 - \theta)I_2/\theta} A_d \omega^2, \quad (65)$$

Therefore, Eq. (55) becomes a condition for θ :

$$\theta > 1 - \frac{I_1^2}{I_2} \equiv \theta_t. \quad (66)$$

Finally, we mention the large-dimension limit of the VDM. For the SDM, we can expand the self-consistent equation, as in Section II C, in the large-dimension limit. To do the same thing for the VDM, we need $\theta \ll 1$ rather than $d \gg 1$. Therefore, the large-dimension limits of the SDM and VDM do not necessarily correspond.

C. Model with continuously vanishing stiffness

In the analysis of the SDM, we implicitly assume that the effective stiffness at zero frequency does not vanish, $k_{\text{eff}}(0) \neq 0$. However, when the probability distribution $P(k_\alpha)$ has a divergence at $k_\alpha = 0$, the effective stiffness can be zero. The divergent distribution can be observed in jammed systems, with their initial stress ignored [54]. Because the QLVs disappear when we ignore the initial stress [25, 60], it is interesting to consider the divergent distributions. The most notable example is the percolation problem [40, 45, 55, 61] with the Bernoulli distribution

$$P(k_\alpha) = p\delta(k_\alpha - 1) + (1 - p)\delta(k_\alpha), \quad (67)$$

In this case, the effective stiffness vanishes linearly as $k_{\text{eff}}(0) \sim p - \theta$.

Here, we present another probability distribution that yields a vanishing stiffness. We analyze

$$P(k_\alpha) = \begin{cases} C k_\alpha^{-\gamma} & k_\alpha \in [0, k_{\text{max}}], \\ 0 & \text{otherwise,} \end{cases}, \quad (68)$$

where $0 < \gamma < 1$ and $C = (1 - \gamma)k_{\text{max}}^{\gamma-1}$. We focus on the zero-frequency limit, and Eq. (62) becomes

$$\frac{1}{k_\alpha + (1 - \theta)k_{\text{eff}}(0)/\theta} = \frac{\theta}{k_{\text{eff}}(0)}. \quad (69)$$

In this model, we consider θ as a control parameter and establish that $k_{\text{eff}}(0) \rightarrow 0$ as $\theta \rightarrow 1$. The left-hand side of the equation is

$$\begin{aligned} & \frac{1}{k_\alpha + (1 - \theta)k_{\text{eff}}(0)/\theta}, \\ &= C \int_0^{k_{\text{max}}} \frac{k_\alpha^{-\gamma} dk_\alpha}{k_\alpha + (1 - \theta)k_{\text{eff}}(0)/\theta}, \\ &= C \left[\frac{1 - \theta}{\theta} k_{\text{eff}}(0) \right]^{1-\gamma} \int_0^{k_{\text{max}}\theta/(1-\theta)k_{\text{eff}}(0)} \frac{t^{-\gamma}}{t+1} dt, \\ &\simeq C \left[\frac{1 - \theta}{\theta} k_{\text{eff}}(0) \right]^{1-\gamma} \int_0^\infty \frac{t^{-\gamma}}{t+1} dt, \end{aligned} \quad (70)$$

Therefore, we obtain the effective stiffness at zero frequency:

$$k_{\text{eff}}(0) \sim (1 - \theta)^{\frac{\gamma}{1-\gamma}}, \quad (71)$$

Further, we numerically solved Eq. (69), and Fig. 5 presents the effective stiffness as a function of $1 - \theta$ with $\gamma = 0.1, 0.2, 0.3, 0.4, 0.5, 0.6$, and 0.7 . The solid line represents Eq. (71) with $\gamma = 0.5$, whereas the dotted line represents Eq. (71) with $\gamma = 0.7$.

IV. SUMMARY AND DISCUSSION

In this study, we extended the analysis conducted in the preceding study [51] and derived new results for local instability. In the first part of this paper, we analyzed the SDM, which is one of the simplest elasticity models, using the EMA. We first considered the large-dimension limit, where the EMA becomes exact [53] and established that the model yields the gapless non-Debye scaling law, $g(\omega) \sim \omega^2$, when the system is marginally stable. Therefore, the non-Debye scaling and the associated conventional instability originate from the purely mean-field nature. Next, we analyzed the SDM with specific distributions of stiffness, uniform distribution, and Gaussian distribution. The uniform distribution yields almost the same results as in the case of the large-dimension limit,

even in relatively small dimensions, whereas the Gaussian distribution leads to an unstable solution.

Considering the difference between the uniform and Gaussian distributions, we introduced local instability and discussed its relationship with the QLVs. In particular, we recognized similarities in the size and the energetics between the cores of the QLVs and the response to a local dipolar force. In real amorphous solids, the size of these cores is larger than the microscopic particle size, whereas it suffices to consider one spring in our elasticity models. From this consideration, we expect that the appropriate coarse-graining length for the elasticity theory of amorphous solids is the size of the QLVs [29]. That is, once we coarse-grain the atomistic system to the size of the QLVs, it reduces to the elasticity model. In contrast, for scales below this length scale, we have to consider the microscopic motions of the constituent particles.

It should be noted that there may be other types of instabilities in addition to the local and conventional instabilities under the EMA. We cannot prove that conventional instability always occurs when we avoid local instability. However, as described in Sections II C and II D, the imaginary part arises as the solution of the quadratic self-consistent equation in the case of conventional instability. This is quite general as long as we can expand the equation in a series. When we go beyond the EMA, the combinations of transfer matrices yield many other types of instabilities. However, numerical or experimental studies have not detected such complicated instabilities in real glasses. Therefore, we expect that the elasticity theory with quenched disorder under the EMA is a suitable framework for describing amorphous solids and that higher-order terms in Eq. (6) do not significantly improve our understanding.

Having introduced the local instability, we illustrated that the tail of the stiffness distribution needs to decay more rapidly than linearly with $(k + k_{\min})$ to avoid local instability. Based on this result, we considered the Bates distribution, which covers a wide range of distributions for the stiffness, and illustrated that the SDM with the Bates distribution is destabilized by the local instability as well as the conventional instability, depending on the specific shape of the distribution. We also illustrated that when the system is on the verge of local instability, the vDOS follows another power law: $g_{\text{local}}(\omega) \sim \omega^{2\nu+1}$, where $\nu > 1$ is the exponent of the distribution. This is consistent with the exponent of the vDOS of the QLVs $3 \lesssim \beta \leq 4$ [32], as mentioned in the Introduction.

In the second part of the paper, we discussed the VDM. Here, it should be noted that in Refs. [41, 46], the initial stress was considered the source of the instability of the VDM. Specifically, we consider the term

$-\frac{f_\alpha}{|r_\alpha|} |\alpha\rangle (\hat{\delta}_d - \mathbf{n}_\alpha \otimes \mathbf{n}_\alpha) \langle \alpha|$, where f_α is the force between a pair α in the dynamical matrix. Although we have neglected the initial stress in this study, the mechanism of the local instability is general and valid even when the initial stress is considered. In this case, the distribution of f_α plays a central role. We also presented a class of distributions that yielded the continuously vanishing elastic modulus. By tuning the parameter in the distributions, we can change the scale of the elastic modulus.

Throughout the present analyses on two types of elasticity models, our main finding is that in finite spatial dimensions, local instability can occur. Remarkably, the unstable modes induced by the local instability share characteristic features with the QLV modes, lying in the low-frequency edge of amorphous solids. In addition, although the conventional instability robustly produces the non-Debye quadratic law of $g(\omega) \propto \omega^2$, the quartic law of $g(\omega) \propto \omega^4$, which has been observed in many finite-dimensional systems [22, 24–26, 62, 63], can be rationalized in terms of local instability. We therefore propose that finite-dimensional amorphous solids can occur in a marginally stable state in terms of local instability.

The local nature of marginal stability is also consistent with numerical observations that amorphous solids undergo *local* rearrangements under mechanical loading or thermal agitation [34, 35] that involve 10 to 1000 particles. Experimentally, it is rather difficult to directly observe these microscopic phenomena in samples of materials. However, they can be detected indirectly through experimental measurements. For example, the dependence of heat capacity on linear temperature or that of heat conductivity on squared temperature [9, 12, 64] is considered to be caused by localized transitions through the quantum tunneling mechanism, the so-called two-level systems [10, 11, 64].

In future work, it will be interesting to investigate the effects of anharmonicity or the correlation of the local elastic modulus. The former is necessary to directly study the yielding transition [16–18, 34] and the thermal properties of glasses [9–15]. Recently, the phenomenological theory has been proposed to derive the vDOS of the QLVs by treating the anharmonicity [65]. The latter has been discussed for several decades and has some implications for phonon transport [66, 67]; its understanding has been advanced by recent numerical simulations [68–70].

ACKNOWLEDGMENTS

This work was supported by JSPS KAKENHI Grant Numbers 19J20036, 17H04853, 18H05225, 18H03675, 19H01812, 19K14670, 20H01868, and 20H00128. It was also partially supported by the Asahi Glass Foundation.

Appendix A: Approximation of Green's function in large-dimension limit

In this appendix, we derive Eq. (28) using the Debye approximation. Introducing polar coordinates, $G(\omega)$ is written as follows:

$$\begin{aligned}
G(\omega) &= \int_{0 < |\mathbf{q}| < q_D} \frac{d\mathbf{q}}{(2\pi)^d} \frac{1}{k_{\text{eff}}(\omega) \mathbf{q}^2 - \omega^2}, \\
&= \frac{S_{d-1}}{(2\pi)^d} \int_0^{q_D} dq \frac{q^{d-1}}{k_{\text{eff}}(\omega) q^2 - \omega^2}, \\
&= \frac{S_{d-1} q_D^d}{(2\pi)^d} \int_0^1 dq \frac{q^{d-1}}{k_{\text{eff}}(\omega) q_D^2 q^2 - \omega^2}, \\
&= \frac{d}{k_{\text{eff}}(\omega) q_D^2} \int_0^1 dq \frac{q^{d-1}}{q^2 - \omega^2 / k_{\text{eff}}(\omega) q_D^2},
\end{aligned} \tag{A1}$$

We have used Eq. (13) in the last line. Because an expansion in powers of frequency is convenient to us, the integrand is expanded as follows:

$$\frac{q^{d-1}}{q^2 - \omega^2 / k_{\text{eff}}(\omega) q_D^2} = \begin{cases} \sum_{n=0}^{D-1} q^{2D-2-2n} \left[\frac{\omega^2}{k_{\text{eff}}(\omega) q_D^2} \right]^n + \frac{1}{q^2 - \omega^2 / k_{\text{eff}}(\omega) q_D^2} \left[\frac{\omega^2}{k_{\text{eff}}(\omega) q_D^2} \right]^D & (d = 2D + 1, D = 1, 2, \dots) \\ \sum_{n=0}^{D-1} q^{2D-1-2n} \left[\frac{\omega^2}{k_{\text{eff}}(\omega) q_D^2} \right]^n + \frac{q}{q^2 - \omega^2 / k_{\text{eff}}(\omega) q_D^2} \left[\frac{\omega^2}{k_{\text{eff}}(\omega) q_D^2} \right]^D & (d = 2D + 2, D = 1, 2, \dots) \end{cases}. \tag{A2}$$

At $d \gg 1$, we can neglect the second terms in both cases:

$$\int_0^1 dq \frac{q^{d-1}}{q^2 - \omega^2 / k_{\text{eff}}(\omega) q_D^2} \simeq \begin{cases} \sum_{n=0}^{D-1} \frac{1}{d-2-2n} \left[\frac{\omega^2}{k_{\text{eff}}(\omega) q_D^2} \right]^n & (d = 2D + 1, D = 1, 2, \dots) \\ \sum_{n=0}^{D-1} \frac{1}{d-2-2n} \left[\frac{\omega^2}{k_{\text{eff}}(\omega) q_D^2} \right]^n & (d = 2D + 2, D = 1, 2, \dots) \end{cases}. \tag{A3}$$

We only need the expression that is valid in the low-frequency region. Thus, we approximate $1/(d-2-2n) \sim 1/d$, and therefore,

$$G(\omega) = \frac{d}{k_{\text{eff}}(\omega) q_D^2} \int_0^1 dq \frac{q^{d-1}}{q^2 - \omega^2 / k_{\text{eff}}(\omega) q_D^2} \simeq \frac{1}{k_{\text{eff}}(\omega) q_D^2} \sum_{n=0}^{\infty} \left[\frac{\omega^2}{k_{\text{eff}}(\omega) q_D^2} \right]^n = \frac{1}{k_{\text{eff}}(\omega) q_D^2 - \omega^2}. \tag{A4}$$

Appendix B: Solution for uniform distribution

In this appendix, we solve Eq. (29). To solve the cubic equation, we substitute $k_{\text{eff}}(\omega) = y + \mu/3$,

$$\begin{aligned}
&k_{\text{eff}}(\omega)^3 - \mu k_{\text{eff}}(\omega)^2 + \frac{\sigma^2}{d} k_{\text{eff}}(\omega) + \frac{\sigma^2}{d} A_d \omega^2, \\
&= \left(y + \frac{\mu}{3} \right)^3 - \mu \left(y + \frac{\mu}{3} \right)^2 + \frac{\sigma^2}{d} \left(y + \frac{\mu}{3} \right) + \frac{\sigma^2}{d} A_d \omega^2, \\
&= y^3 + \left(\frac{\mu^2}{3} - \frac{2\mu^2}{3} + \frac{\sigma^2}{d} \right) y + \frac{\mu^3}{27} - \frac{\mu^3}{9} + \mu \frac{\sigma^2}{3d} + \frac{\sigma^2}{d} A_d \omega^2, \\
&= y^3 + \left(-\frac{\mu^2}{3} + \frac{\sigma^2}{d} \right) y - \frac{2\mu^3}{27} + \mu \frac{\sigma^2}{3d} + \frac{\sigma^2}{d} A_d \omega^2, \\
&= y^3 + 3 \left(-\frac{\mu^2}{9} + \frac{\sigma^2}{3d} \right) y + 2 \left(-\frac{\mu^3}{27} + \mu \frac{\sigma^2}{6d} + \frac{\sigma^2}{2d} A_d \omega^2 \right), \\
&\equiv y^3 + 3Py + 2Q.
\end{aligned} \tag{B1}$$

Using the critical value defined in the preceding section, $\sigma_c = \sqrt{d}\mu/2$, P can be written as follows:

$$\begin{aligned}
P &= -\frac{\mu^2}{9} + \frac{\sigma^2}{3d}, \\
&= -\frac{\mu^2}{9} + \frac{\sigma_c^2}{3d} - \frac{\sigma_c^2 - \sigma^2}{3d}. \\
&= -\frac{\mu^2}{36} - \frac{\sigma_c^2 - \sigma^2}{3d} \\
&= -\left(\frac{\mu}{6}\right)^2 - \frac{\sigma_c^2 - \sigma^2}{3d}, \\
&\equiv -\left(\frac{\mu}{6}\right)^2 - \frac{\delta_\sigma^2}{3d}.
\end{aligned} \tag{B2}$$

Therefore, Q becomes

$$\begin{aligned}
Q &= -\frac{\mu^3}{27} + \mu\frac{\sigma^2}{6d} + \frac{\sigma^2}{2d}A_d\omega^2, \\
&= -\frac{\mu^3}{27} + \mu\frac{\sigma_c^2}{6d} - \mu\frac{\sigma_c^2 - \sigma^2}{6d} + \frac{\sigma^2}{2d}A_d\omega^2, \\
&= \left(-\frac{1}{27} + \frac{1}{24}\right)\mu^3 - \mu\frac{\sigma_c^2 - \sigma^2}{6d} + \frac{\sigma^2}{2d}A_d\omega^2, \\
&= \left(\frac{\mu}{6}\right)^3 - \mu\frac{\sigma_c^2 - \sigma^2}{6d} + \frac{\sigma^2}{2d}A_d\omega^2. \\
&\equiv \left(\frac{\mu}{6}\right)^3 - \frac{\mu\delta_\sigma^2}{6d} + \frac{\sigma^2}{2d}A_d\omega^2.
\end{aligned} \tag{B3}$$

To discuss the vibrations at $\sigma \lesssim \sigma_c$, we set $\delta_\sigma^2/\mu^2 \sim \omega^2/\mu \ll 1$ and derive approximate expressions for $k_{\text{eff}}(\omega)$. Therefore, Q can be approximated as follows:

$$Q \simeq \left(\frac{\mu}{6}\right)^3 - \frac{\mu\delta_\sigma^2}{6d} + \frac{\sigma_c^2}{2d}A_d\omega^2. \tag{B4}$$

Next, we need to compute

$$\left(-Q \pm \sqrt{Q^2 + P^3}\right)^{1/3}. \tag{B5}$$

Let us treat the terms under the square root:

$$\begin{aligned}
&Q^2 + P^3 \\
&\simeq \left[\left(\frac{\mu}{6}\right)^3 - \frac{\mu\delta_\sigma^2}{6d} + \frac{\sigma_c^2}{2d}A_d\omega^2\right]^2 - \left[\left(\frac{\mu}{6}\right)^2 + \frac{\delta_\sigma^2}{3d}\right]^3, \\
&= \left(\frac{\mu}{6}\right)^6 - 2\left(\frac{\mu}{6}\right)^3\frac{\mu\delta_\sigma^2}{6d} + \left(\frac{\mu\delta_\sigma^2}{6d}\right)^2 + \frac{\sigma_c^2}{2d}A_d\omega^2\left\{\frac{\sigma_c^2}{2d}A_d\omega^2 + 2\left[\left(\frac{\mu}{6}\right)^3 - \mu\frac{\delta_\sigma^2}{6d}\right]\right\}, \\
&\quad - \left[\left(\frac{\mu}{6}\right)^6 + 3\left(\frac{\mu}{6}\right)^4\frac{\delta_\sigma^2}{3d} + 3\left(\frac{\mu}{6}\right)^2\left(\frac{\delta_\sigma^2}{3d}\right)^2 + \left(\frac{\delta_\sigma^2}{3d}\right)^3\right]. \\
&= -3\left(\frac{\mu}{6}\right)^4\frac{\delta_\sigma^2}{d} + \frac{2}{3}\left(\frac{\mu\delta_\sigma^2}{6d}\right)^2 + \frac{1}{4}\left(\frac{\sigma_c^2}{d}A_d\omega^2\right)^2 + \left(\frac{\mu}{6}\right)^3\frac{\sigma_c^2}{d}A_d\omega^2 - \frac{\mu\delta_\sigma^2}{6d}\frac{\sigma_c^2}{d}A_d\omega^2 \\
&\simeq -3\left(\frac{\mu}{6}\right)^4\frac{\delta_\sigma^2}{d} + \left(\frac{\mu}{6}\right)^3\frac{\sigma_c^2}{d}A_d\omega^2, \\
&= -3\left(\frac{\mu}{6}\right)^4\frac{\delta_\sigma^2}{d} + \left(\frac{\mu}{6}\right)^3\frac{\mu^2}{4}A_d\omega^2, \\
&= 9\left(\frac{\mu}{6}\right)^5\left(A_d\omega^2 - 2\frac{\delta_\sigma^2}{d\mu}\right),
\end{aligned} \tag{B6}$$

Therefore,

$$\begin{aligned}
& \left(-Q \pm \sqrt{Q^2 + P^3}\right)^{1/3} \\
& \simeq \left[\left(-\frac{\mu}{6}\right)^3 + \frac{\mu\delta_\sigma^2}{6d} - \frac{\sigma_c^2}{2d}A_d\omega^2 \pm \sqrt{9\left(\frac{\mu}{6}\right)^5\left(A_d\omega^2 - 2\frac{\delta_\sigma^2}{d\mu}\right)} \right]^{1/3}, \\
& \simeq \left[\left(-\frac{\mu}{6}\right)^3 \pm \sqrt{9\left(\frac{\mu}{6}\right)^5\left(A_d\omega^2 - 2\frac{\delta_\sigma^2}{d\mu}\right)} \right]^{1/3}, \\
& = -\frac{\mu}{6} \left[1 \pm 3\frac{-6}{\mu}\sqrt{\frac{\mu}{6}\left(A_d\omega^2 - 2\frac{\delta_\sigma^2}{d\mu}\right)} \right]^{1/3}, \\
& \simeq -\frac{\mu}{6} \left[1 \pm \frac{-6}{\mu}\sqrt{\frac{\mu}{6}\left(A_d\omega^2 - 2\frac{\delta_\sigma^2}{d\mu}\right)} \right], \\
& = -\frac{\mu}{6} \pm \sqrt{\frac{\mu}{6}\left(A_d\omega^2 - 2\frac{\delta_\sigma^2}{d\mu}\right)},
\end{aligned} \tag{B7}$$

We choose a solution that satisfies $k_{\text{eff}}(0) \rightarrow \mu$ as $\sigma \rightarrow 0$ and $\Sigma(\omega) \equiv -\text{Im} k_{\text{eff}}(\omega) < 0$. Thus, we obtain

$$\begin{aligned}
k_{\text{eff}}(\omega) - \frac{\mu}{3} &= \frac{-1 - \sqrt{3}i}{2} \left(-Q + \sqrt{Q^2 + P^3}\right)^{1/3} + \frac{-1 + \sqrt{3}i}{2} \left(-Q - \sqrt{Q^2 + P^3}\right)^{1/3}, \\
k_{\text{eff}}(\omega) &\simeq \frac{\mu}{3} + \frac{-1 - \sqrt{3}i}{2} \left[-\frac{\mu}{6} + \sqrt{\frac{\mu}{6}\left(A_d\omega^2 - 2\frac{\delta_\sigma^2}{d\mu}\right)}\right] + \frac{-1 + \sqrt{3}i}{2} \left[-\frac{\mu}{6} - \sqrt{\frac{\mu}{6}\left(A_d\omega^2 - 2\frac{\delta_\sigma^2}{d\mu}\right)}\right], \\
&= \frac{\mu}{2} - i\sqrt{\frac{\mu}{2}\left(A_d\omega^2 - 2\frac{\delta_\sigma^2}{d\mu}\right)}, \\
&\equiv \frac{\mu}{2} - i\sqrt{\frac{\mu}{2}\sqrt{A_d\omega^2 - A_d\omega_0'^2}},
\end{aligned} \tag{B8}$$

Appendix C: Asymptotic solution for Gaussian distribution in large-dimension limit

In this appendix, we derive Eqs. (36) and (37). At $\sigma < \sigma_c$ and $d \rightarrow \infty$, we can assume that $k_r(0) \gg \Sigma(0)$. Therefore, linearizing Eq. (35) around $\Sigma(0)$, we obtain

$$\begin{aligned}
F\left[\frac{\mu + (d-1)k_r(0)}{\sqrt{2}\sigma}\right] + F'\left[\frac{\mu + (d-1)k_r(0)}{\sqrt{2}\sigma}\right] \left[-i\frac{(d-1)\Sigma(0)}{\sqrt{2}\sigma}\right] + i\frac{\sqrt{\pi}}{2} \exp\left\{-\frac{[\mu + (d-1)k_r(0)]^2}{2\sigma^2}\right\}, \\
- \frac{\sqrt{\pi}(d-1)[\mu + (d-1)]}{2\sigma^2} \exp\left\{-\frac{[\mu + (d-1)k_r(0)]^2}{2\sigma^2}\right\}, \Sigma(0) \simeq \frac{\sigma}{\sqrt{2}dk_r(0)} + i\frac{\sigma\Sigma(0)}{\sqrt{2}dk_r(0)^2}
\end{aligned} \tag{C1}$$

We use the differential equation satisfied by the Dawson function $F'(z) + 2zF(z) = 1$ and the asymptotic expansion:

$$F(z) = \sum_{k=0}^{\infty} \frac{(2k-1)!!}{2^{k+1}z^{2k+1}} = \frac{1}{2z} + \frac{1}{4z^3} + \frac{3}{8z^5} + \dots \text{ as } |z| \rightarrow \infty. \tag{C2}$$

The left-hand side of Eq. (C1) is

$$\begin{aligned}
& F \left[\frac{\mu + (d-1)k_r(0)}{\sqrt{2}\sigma} \right] + F' \left[\frac{\mu + (d-1)k_r(0)}{\sqrt{2}\sigma} \right] \left[-i \frac{(d-1)\Sigma(0)}{\sqrt{2}\sigma} \right], \\
& = F \left[\frac{\mu + (d-1)k_r(0)}{\sqrt{2}\sigma} \right] + \left\{ 1 - 2 \frac{\mu + (d-1)k_r(0)}{\sqrt{2}\sigma} F \left[\frac{\mu + (d-1)k_r(0)}{\sqrt{2}\sigma} \right] \right\} \left[-i \frac{(d-1)\Sigma(0)}{\sqrt{2}\sigma} \right], \\
& \simeq \frac{1}{2} \frac{\sqrt{2}\sigma}{\mu + (d-1)k_r(0)} + \frac{1}{4} \left[\frac{\sqrt{2}\sigma}{\mu + (d-1)k_r(0)} \right]^3, \\
& - 2 \frac{\mu + (d-1)k_r(0)}{\sqrt{2}\sigma} \left\{ \frac{1}{4} \left[\frac{\sqrt{2}\sigma}{\mu + (d-1)k_r(0)} \right]^3 + \frac{3}{8} \left[\frac{\sqrt{2}\sigma}{\mu + (d-1)k_r(0)} \right]^5 \right\} \left[-i \frac{(d-1)\Sigma(0)}{\sqrt{2}\sigma} \right].
\end{aligned} \tag{C3}$$

The real part of Eq. (C1) is

$$\begin{aligned}
& \frac{1}{2} \frac{\sqrt{2}\sigma}{\mu + (d-1)k_r(0)} + \frac{1}{4} \left[\frac{\sqrt{2}\sigma}{\mu + (d-1)k_r(0)} \right]^3 = \frac{\sigma}{\sqrt{2}dk_r(0)} \\
& \frac{1}{\mu + (d-1)k_r(0)} + \frac{\sigma^2}{[\mu + (d-1)k_r(0)]^3} = \frac{1}{dk_r(0)} \\
& \frac{k_r(0) - \mu}{dk_r(0) [\mu + (d-1)k_r(0)]} + \frac{\sigma^2}{[\mu + (d-1)k_r(0)]^3} = 0.
\end{aligned} \tag{C4}$$

Because $k_r(0) = \mathcal{O}(1)$ in the large-dimension limit, this is simplified to

$$\begin{aligned}
& \frac{k_r(0) - \mu}{d^2 k_r(0)^2} + \frac{\sigma^2}{d^3 k_r(0)^3} = 0 \\
& dk_r(0)^2 - \mu dk_r(0) + \sigma^2 = 0.
\end{aligned} \tag{C5}$$

Therefore, the real part is

$$k_r(0) = \frac{\mu}{2} + \frac{1}{2} \sqrt{\mu^2 - 4 \frac{\sigma^2}{d}}, \tag{C6}$$

which is essentially the same as Eq. (21). The imaginary part of Eq. (C1) is

$$\begin{aligned}
& -2 \frac{\mu + (d-1)k_r(0)}{\sqrt{2}\sigma} \left[\frac{1}{4} \left(\frac{\sqrt{2}\sigma}{\mu + (d-1)k_r(0)} \right)^3 + \frac{3}{8} \left(\frac{\sqrt{2}\sigma}{\mu + (d-1)k_r(0)} \right)^5 \right] \left[-\frac{(d-1)\Sigma(0)}{\sqrt{2}\sigma} \right] \\
& + \frac{\sqrt{\pi}}{2} \exp \left\{ -\frac{[\mu + (d-1)k_r(0)]^2}{2\sigma^2} \right\} = \frac{\sigma \Sigma(0)}{\sqrt{2}dk_r(0)^2}, \\
& \frac{\sigma}{\sqrt{2}} \left\{ \frac{\mu^2 + 2\mu(d-1)k_r(0) - (d-1)k_r(0)^2}{dk_r(0)^2 [\mu + (d-1)k_r(0)]^2} - \frac{3(d-1)\sigma^2}{[\mu + (d-1)k_r(0)]^4} \right\} \Sigma(0) = \frac{\sqrt{\pi}}{2} \exp \left\{ -\frac{[\mu + (d-1)k_r(0)]^2}{2\sigma^2} \right\}.
\end{aligned} \tag{C7}$$

Employing the same procedure as in the real part, this can be simplified to

$$\begin{aligned}
& \frac{\sigma}{\sqrt{2}} \left[\frac{2\mu dk_r(0) - dk_r(0)^2}{d^3 k_r(0)^4} - \frac{3d\sigma^2}{d^4 k_r(0)^4} \right] \Sigma(0) = \frac{\sqrt{\pi}}{2} \exp \left[-\frac{d^2 k_r(0)^2}{2\sigma^2} \right] \\
& [2\mu dk_r(0) - dk_r(0)^2 - 3\sigma^2] \Sigma(0) = \frac{d^3 k_r(0)^4}{\sigma} \sqrt{\frac{\pi}{2}} \exp \left[-\frac{d^2 k_r(0)^2}{2\sigma^2} \right] \\
& \left[k_r(0) - 2 \frac{\sigma^2}{\mu d} \right] \Sigma(0) = \frac{d^2 k_r(0)^4}{\mu \sigma} \sqrt{\frac{\pi}{2}} \exp \left[-\frac{d^2 k_r(0)^2}{2\sigma^2} \right] \\
& \Sigma(0) = \sqrt{\frac{\pi}{2}} \frac{d^2 k_r(0)^4 \exp \left[-\frac{d^2 k_r(0)^2}{2\sigma^2} \right]}{\mu \sigma \left[k_r(0) - 2 \frac{\sigma^2}{\mu d} \right]}.
\end{aligned} \tag{C8}$$

To obtain the third line from the second, we have used Eq. (C5).

Appendix D: Marginal solution using local instability

In this appendix, we solve Eq. (50) in the lowest-frequency region. The left-hand side of Eq. (50) can be transformed as

$$\begin{aligned}
& \mathcal{P} \int_{-\Delta}^{\Delta} \frac{dk_{\alpha} P(k_{\alpha} + \mu)}{k_{\alpha} + \mu + (d-1)k_r(\omega) - dA_d\omega^2} \\
&= \mathcal{P} \int_{-1}^1 \frac{dk_{\alpha} \Delta P(\Delta k_{\alpha} + \mu)}{\Delta k_{\alpha} + \mu + (d-1)k_r(\omega) - dA_d\omega^2} \\
&\equiv \mathcal{P} \int_{-1}^1 \frac{dx \tilde{P}(x)}{\Delta k_{\alpha} + \mu + (d-1)k_r(\omega) - dA_d\omega^2}.
\end{aligned} \tag{D1}$$

It should be noted that $\tilde{P}(x)$ is the same distribution as $P(x)$, but it is supported in the interval $[-1, 1]$. We decompose $k_r(\omega)$ as $k_r(\omega) = [-\mu + \Delta + \delta k_r(\omega)]/(d-1)$, and the denominator of the integrand becomes

$$\frac{\Delta + \delta k_r(\omega) - dA_d\omega^2}{\Delta} = 1 - \frac{-\delta k_r(\omega) + dA_d\omega^2}{\Delta} \equiv 1 - \frac{\eta(\omega)}{\Delta}. \tag{D2}$$

We assume that $\delta k_r(\omega), \eta(\omega) \sim \omega^2$ as $\omega \rightarrow 0$. In the following, we expand Eq. (D1) to the first order in ω^2 . Before that, we treat the principal value part of Eq. (D1). Equation (D1) can be expressed as follows:

$$\begin{aligned}
& \frac{1}{\Delta} \mathcal{P} \int_{-1}^1 \frac{dx \tilde{P}(x)}{x + 1 - \eta(\omega)/\Delta} \\
&= \frac{1}{\Delta} \mathcal{P} \int_{-1}^{-1+2\eta(\omega)/\Delta} \frac{dx \tilde{P}(x)}{x + 1 - \eta(\omega)/\Delta} + \frac{1}{\Delta} \int_{-1+2\eta(\omega)/\Delta}^1 \frac{dx \tilde{P}(x)}{x + 1 - \eta(\omega)/\Delta}.
\end{aligned} \tag{D3}$$

Using the assumption $\tilde{P}(x) = (\text{const.})(x+1)^{\nu}$ with $\nu > 1$ at $x \simeq -1$, we can prove that the first term is negligible as follows:

$$\begin{aligned}
& \frac{1}{\Delta} \mathcal{P} \int_{-1}^{-1+2\eta(\omega)/\Delta} \frac{dx \tilde{P}(x)}{x + 1 - \eta(\omega)/\Delta}, \\
&= \frac{\eta(\omega)^{\nu}}{\Delta^{\nu+1}} \mathcal{P} \int_{-1}^{-1+2\eta(\omega)/\Delta} \frac{dx \Delta/\eta(\omega) [(x+1)\Delta/\eta(\omega)]^{\nu}}{(x+1)\Delta/\eta(\omega) - 1}, \\
&= \frac{\eta(\omega)^{\nu}}{\Delta^{\nu+1}} \mathcal{P} \int_0^2 dt \frac{t^{\nu}}{t-1}, \\
&= o(\omega^2),
\end{aligned} \tag{D4}$$

where we ignore the numerical factors during calculation. Now, we expand Eq. (D1) up to the first order in ω^2 as follows:

$$\begin{aligned}
& \frac{1}{\Delta} \mathcal{P} \int_{-1}^1 \frac{dx \tilde{P}(x)}{x + 1 - \eta(\omega)/\Delta} \\
&= \frac{1}{\Delta} \int_{-1+2\eta(\omega)/\Delta}^1 \frac{dx \tilde{P}(x)}{x + 1 - \eta(\omega)/\Delta} + o(\omega^2) \\
&= \frac{1}{\Delta} \int_{-1}^1 \frac{dx \tilde{P}(x)}{x + 1} + \frac{1}{\Delta^2} \int_{-1}^1 dx \frac{\tilde{P}(x)}{(x+1)^2} [-\delta k_r(\omega) + dA_d\omega^2] + o(\omega^2) \\
&\equiv \frac{I_1}{\Delta} + \frac{I_2}{\Delta^2} [-\delta k_r(\omega) + dA_d\omega^2] + o(\omega^2),
\end{aligned} \tag{D5}$$

where

$$I_m \equiv \int_{-1}^1 dx \frac{\tilde{P}(x)}{(x+1)^m}. \tag{D6}$$

The right-hand side of Eq. (50) can also be expanded as

$$\begin{aligned} & \frac{1}{dk_r(\omega)} \left[1 + \frac{A_d \omega^2}{k_r(\omega)} \right] \\ &= \frac{d-1}{d[-\mu + \Delta + \delta k_r(\omega)]} \left[1 + \frac{(d-1)A_d \omega^2}{-\mu + \Delta + \delta k_r(\omega)} \right] \\ &= \frac{d-1}{d(-\mu + \Delta)} + \frac{(d-1)}{d(-\mu + \Delta)^2} [-\delta k_r(\omega) + (d-1)A_d \omega^2] + \mathcal{O}(\omega^4). \end{aligned} \quad (\text{D7})$$

Comparing Eqs. (D5) and (D7), the equation at zero frequency is as follows:

$$I_1 = \frac{\Delta(d-1)}{d(-\mu + \Delta)}. \quad (\text{D8})$$

The equation for $\delta k_r(\omega)$ is as follows:

$$\begin{aligned} \frac{I_2}{\Delta^2} [-\delta k_r(\omega) + dA_d \omega^2] &= \frac{(d-1)}{d(-\mu + \Delta)^2} [-\delta k_r(\omega) + (d-1)A_d \omega^2], \\ I_2 [-\delta k_r(\omega) + dA_d \omega^2] &= \frac{d}{d-1} I_1^2 [-\delta k_r(\omega) + (d-1)A_d \omega^2], \\ \frac{\delta k_r(\omega)}{d-1} &= -\frac{dI_2 - dI_1^2}{dI_1^2 - (d-1)I_2} A_d \omega^2. \end{aligned} \quad (\text{D9})$$

To obtain the second line from the first, we have used Eq. (D8).

-
- [1] C. Kittel. *Introduction to Solid State Physics*. John Wiley and Sons, New York, 7th ed. edition, 1996.
- [2] U. Buchenau, N. Nücker, and A. J. Dianoux. Neutron scattering study of the low-frequency vibrations in vitreous silica. *Phys. Rev. Lett.*, 53:2316–2319, Dec 1984.
- [3] Brian B. Laird and H. R. Schober. Localized low-frequency vibrational modes in a simple model glass. *Phys. Rev. Lett.*, 66:636–639, Feb 1991.
- [4] H. R. Schober and Brian B. Laird. Localized low-frequency vibrational modes in glasses. *Phys. Rev. B*, 44:6746–6754, Oct 1991.
- [5] F. Leonforte, R. Boissière, A. Tanguy, J. P. Wittmer, and J.-L. Barrat. Continuum limit of amorphous elastic bodies. iii. three-dimensional systems. *Phys. Rev. B*, 72:224206, Dec 2005.
- [6] Giulio Monaco and Stefano Mossa. Anomalous properties of the acoustic excitations in glasses on the mesoscopic length scale. *Proceedings of the National Academy of Sciences*, 106(40):16907–16912, 2009.
- [7] S. N. Taraskin and S. R. Elliott. Anharmonicity and localization of atomic vibrations in vitreous silica. *Phys. Rev. B*, 59:8572–8585, Apr 1999.
- [8] N. Xu, V. Vitelli, A. J. Liu, and S. R. Nagel. Anharmonic and quasi-localized vibrations in jammed solids—modes for mechanical failure. *Europhys. Lett.*, 90(5):56001, 2010.
- [9] R. C. Zeller and R. O. Pohl. Thermal conductivity and specific heat of noncrystalline solids. *Phys. Rev. B*, 4:2029–2041, Sep 1971.
- [10] P. W. Anderson, B. I. Halperin, and C. M. Varma. Anomalous low-temperature thermal properties of glasses and spin glasses. *Philosophical Mag.*, 25(1):1–9, 1972.
- [11] W. A. Phillips. Tunneling states in amorphous solids. *J. Low Temp. Phys.*, 7(3):351–360, 1972.
- [12] W.A. Phillips. *Amorphous solids: low-temperature properties*. Topics in current physics. Springer-Verlag, 1981.
- [13] VG Karpov, I Klinger, and FN Ignat’Ev. Theory of the low-temperature anomalies in the thermal properties of amorphous structures. *Zh. Eksp. Teor. Fiz*, 84:760, 1983.
- [14] U. Buchenau, Yu. M. Galperin, V. L. Gurevich, and H. R. Schober. Anharmonic potentials and vibrational localization in glasses. *Phys. Rev. B*, 43:5039–5045, Feb 1991.
- [15] U. Buchenau, Yu. M. Galperin, V. L. Gurevich, D. A. Parshin, M. A. Ramos, and H. R. Schober. Interaction of soft modes and sound waves in glasses. *Phys. Rev. B*, 46:2798–2808, Aug 1992.
- [16] Craig E. Maloney and Anael Lemaitre. Amorphous systems in athermal, quasistatic shear. *Phys. Rev. E*, 74:016118, Jul 2006.
- [17] A. Tanguy, B. Mantisi, and M. Tsamados. Vibrational modes as a predictor for plasticity in a model glass. *Europhys. Lett.*, 90(1):16004, 2010.
- [18] M. L. Manning and A. J. Liu. Vibrational modes identify soft spots in a sheared disordered packing. *Phys. Rev. Lett.*, 107:108302, Aug 2011.
- [19] C. Oligschleger and H. R. Schober. Collective jumps in a soft-sphere glass. *Phys. Rev. B*, 59:811–821, Jan 1999.
- [20] Asaph Widmer-Cooper, Heidi Perry, Peter Harrowell, and David R. Reichman. Localized soft modes and the supercooled liquid’s irreversible passage through its configuration space. *J. Chem. Phys.*, 131(19):194508, 2009.
- [21] Patrick Charbonneau, Eric I. Corwin, Giorgio Parisi, Alexis Poncet, and Francesco Zamponi. Universal non-

- debye scaling in the density of states of amorphous solids. *Phys. Rev. Lett.*, 117:045503, Jul 2016.
- [22] Masanari Shimada, Hideyuki Mizuno, and Atsushi Ikeda. Anomalous vibrational properties in the continuum limit of glasses. *Phys. Rev. E*, 97:022609, Feb 2018.
- [23] Masanari Shimada, Hideyuki Mizuno, Ludovic Berthier, and Atsushi Ikeda. Low-frequency vibrations of jammed packings in large spatial dimensions. *Phys. Rev. E*, 101:052906, May 2020.
- [24] Edan Lerner, Gustavo Düring, and Eran Bouchbinder. Statistics and properties of low-frequency vibrational modes in structural glasses. *Phys. Rev. Lett.*, 117:035501, Jul 2016.
- [25] Hideyuki Mizuno, Hayato Shiba, and Atsushi Ikeda. Continuum limit of the vibrational properties of amorphous solids. *Proc. Natl. Acad. Sci. U.S.A.*, 114(46):E9767–E9774, 2017.
- [26] Lijin Wang, Andrea Ninarello, Pengfei Guan, Ludovic Berthier, Grzegorz Szamel, and Elijah Flenner. Low-frequency vibrational modes of stable glasses. *Nature Communications*, 10:26, 2019.
- [27] Luka Gartner and Edan Lerner. Nonlinear plastic modes in disordered solids. *Phys. Rev. E*, 93:011001, Jan 2016.
- [28] Masanari Shimada, Hideyuki Mizuno, Matthieu Wyart, and Atsushi Ikeda. Spatial structure of quasilocated vibrations in nearly jammed amorphous solids. *Phys. Rev. E*, 98:060901, Dec 2018.
- [29] Edan Lerner, Eric DeGiuli, Gustavo Düring, and Matthieu Wyart. Breakdown of continuum elasticity in amorphous solids. *Soft Matter*, 10:5085–5092, 2014.
- [30] Le Yan, Eric DeGiuli, and Matthieu Wyart. On variational arguments for vibrational modes near jamming. *EPL (Europhysics Letters)*, 114(2):26003, 2016.
- [31] Edan Lerner and Eran Bouchbinder. A characteristic energy scale in glasses. *The Journal of Chemical Physics*, 148(21):214502, 2018.
- [32] Edan Lerner and Eran Bouchbinder. Effect of instantaneous and continuous quenches on the density of vibrational modes in model glasses. *Phys. Rev. E*, 96:020104, Aug 2017.
- [33] Markus Müller and Matthieu Wyart. Marginal stability in structural, spin, and electron glasses. *Annual Review of Condensed Matter Physics*, 6(1):177–200, 2015.
- [34] Smarajit Karmakar, Edan Lerner, and Itamar Procaccia. Statistical physics of the yielding transition in amorphous solids. *Phys. Rev. E*, 82:055103, Nov 2010.
- [35] Hideyuki Mizuno, Masanari Shimada, and Atsushi Ikeda. Anharmonic properties of vibrational excitations in amorphous solids. *Phys. Rev. Research*, 2:013215, Feb 2020.
- [36] Matthieu Wyart, Leonardo E. Silbert, Sidney R. Nagel, and Thomas A. Witten. Effects of compression on the vibrational modes of marginally jammed solids. *Phys. Rev. E*, 72:051306, Nov 2005.
- [37] In general, the concept of marginal stability requires understanding other phenomena, including crackling in a finite range of external fields [33]. We do not consider these related topics in this paper.
- [38] W. Schirmacher. Thermal conductivity of glassy materials and the “boson peak”. *Europhys. Lett.*, 73:892, 2006.
- [39] W. Schirmacher, G. Ruocco, and T. Scopigno. Acoustic attenuation in glasses and its relation with the boson peak. *Phys. Rev. Lett.*, 98:025501, 2007.
- [40] M. Wyart. Scaling of phononic transport with connectivity in amorphous solids. *EPL (Europhysics Letters)*, 89(6):64001, 2010.
- [41] Eric DeGiuli, Adrien Laversanne-Finot, Gustavo Düring, Edan Lerner, and Matthieu Wyart. Effects of coordination and pressure on sound attenuation, boson peak and elasticity in amorphous solids. *Soft Matter*, 10:5628–5644, 2014.
- [42] Silvio Franz, Giorgio Parisi, Pierfrancesco Urbani, and Francesco Zamponi. Universal spectrum of normal modes in low-temperature glasses. *Proceedings of the National Academy of Sciences*, 112(47):14539–14544, 2015.
- [43] Harukuni Ikeda. Note: Effect of localization on mean-field density of state near jamming, 2018.
- [44] Harukuni Ikeda. Universal non-mean-field scaling in the density of state of amorphous solids, 2018.
- [45] Gustavo Düring, Edan Lerner, and Matthieu Wyart. Phonon gap and localization lengths in floppy materials. *Soft Matter*, 9:146–154, 2013.
- [46] Eric DeGiuli, Edan Lerner, Carolina Brito, and Matthieu Wyart. Force distribution affects vibrational properties in hard-sphere glasses. *Proceedings of the National Academy of Sciences*, 111(48):17054–17059, 2014.
- [47] Corey S. O’Hern, Stephen A. Langer, Andrea J. Liu, and Sidney R. Nagel. Random packings of frictionless particles. *Phys. Rev. Lett.*, 88:075507, Jan 2002.
- [48] Corey S. O’Hern, Leonardo E. Silbert, Andrea J. Liu, and Sidney R. Nagel. Jamming at zero temperature and zero applied stress: The epitome of disorder. *Phys. Rev. E*, 68:011306, Jul 2003.
- [49] Leonardo E. Silbert, Andrea J. Liu, and Sidney R. Nagel. Vibrations and diverging length scales near the unjamming transition. *Phys. Rev. Lett.*, 95:098301, Aug 2005.
- [50] Leonardo E. Silbert, Andrea J. Liu, and Sidney R. Nagel. Normal modes in model jammed systems in three dimensions. *Phys. Rev. E*, 79:021308, Feb 2009.
- [51] Masanari Shimada, Hideyuki Mizuno, and Atsushi Ikeda. Vibrational spectrum derived from local mechanical response in disordered solids. *Soft Matter*, 16:7279–7288, 2020.
- [52] S. Köhler, G. Ruocco, and W. Schirmacher. Coherent potential approximation for diffusion and wave propagation in topologically disordered systems. *Phys. Rev. B*, 88:064203, Aug 2013.
- [53] J. M. Luck. Conductivity of random resistor networks: An investigation of the accuracy of the effective-medium approximation. *Phys. Rev. B*, 43:3933–3944, Feb 1991.
- [54] Hideyuki Mizuno, Kuniyasu Saitoh, and Leonardo E. Silbert. Elastic moduli and vibrational modes in jammed particulate packings. *Phys. Rev. E*, 93:062905, Jun 2016.
- [55] Shechao Feng and Pabitra N. Sen. Percolation on elastic networks: New exponent and threshold. *Phys. Rev. Lett.*, 52:216–219, Jan 1984.
- [56] Carolina Brito and Matthieu Wyart. Geometric interpretation of previtrification in hard sphere liquids. *The Journal of Chemical Physics*, 131(2):024504, 2009.
- [57] Hideyuki Mizuno, Leonardo E. Silbert, and Matthias Sperl. Spatial distributions of local elastic moduli near the jamming transition. *Phys. Rev. Lett.*, 116:068302, Feb 2016.
- [58] S N Taraskin and S R Elliott. Vector vibrations and the ioffe-regel crossover in disordered lattices. *Journal of Physics: Condensed Matter*, 15(13):2233–2233, mar 2003.

- [59] As $d \rightarrow \infty$, $\sigma_0 \rightarrow \sigma_c \equiv \sqrt{d}\mu/2$ as described in Section II C.
- [60] Edan Lerner and Eran Bouchbinder. Frustration-induced internal stresses are responsible for quasilocalized modes in structural glasses. *Phys. Rev. E*, 97:032140, Mar 2018.
- [61] Shechao Feng, M. F. Thorpe, and E. Garboczi. Effective-medium theory of percolation on central-force elastic networks. *Phys. Rev. B*, 31:276–280, Jan 1985.
- [62] David Richard, Karina González-López, Geert Kapteijns, Robert Pater, Talya Vaknin, Eran Bouchbinder, and Edan Lerner. Universality of the nonphononic vibrational spectrum across different classes of computer glasses, 2020.
- [63] Prasenjit Das, H. George E. Hentschel, Edan Lerner, and Itamar Procaccia. Robustness of density of low-frequency states in amorphous solids. *Phys. Rev. B*, 102:014202, Jul 2020.
- [64] Tomás Pérez-Castañeda, Rafael J. Jiménez-Rioboo, and Miguel A. Ramos. Two-level systems and boson peak remain stable in 110-million-year-old amber glass. *Phys. Rev. Lett.*, 112:165901, 2014.
- [65] Wencheng Ji, Marko Popović, Tom W. J. de Geus, Edan Lerner, and Matthieu Wyart. Theory for the density of interacting quasilocalized modes in amorphous solids. *Phys. Rev. E*, 99:023003, Feb 2019.
- [66] Sajeev John and Michael J. Stephen. Wave propagation and localization in a long-range correlated random potential. *Phys. Rev. B*, 28:6358–6368, Dec 1983.
- [67] Bingyu Cui and Alessio Zaccone. Analytical theory of enhanced logarithmic rayleigh scattering in amorphous solids, 2019.
- [68] Hideyuki Mizuno and Atsushi Ikeda. Phonon transport and vibrational excitations in amorphous solids. *Phys. Rev. E*, 98:062612, Dec 2018.
- [69] Lijin Wang, Ludovic Berthier, Elijah Flenner, Pengfei Guan, and Grzegorz Szamel. Sound attenuation in stable glasses. *Soft Matter*, 15:7018–7025, 2019.
- [70] Avraham Moriel, Geert Kapteijns, Corrado Rainone, Jacques Zylberg, Edan Lerner, and Eran Bouchbinder. Wave attenuation in glasses: Rayleigh and generalized-rayleigh scattering scaling. *The Journal of Chemical Physics*, 151(10):104503, 2019.